Active Galactic Nuclei

Introduction

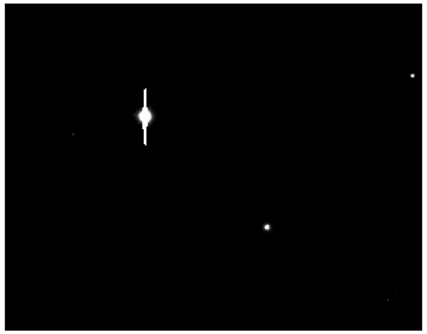

NGC 3783: *linear* intensity scale

Introduction

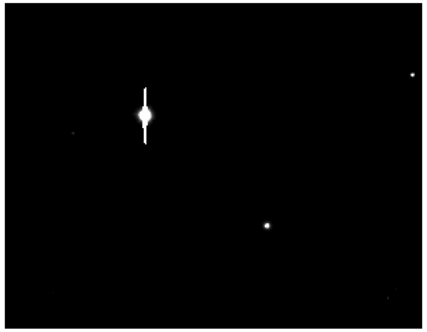

NGC 3783: *linear* intensity scale

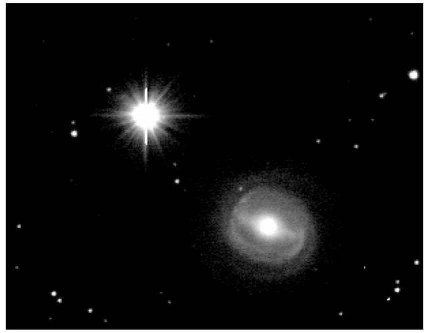

logarithmic intensity scale

Introduction

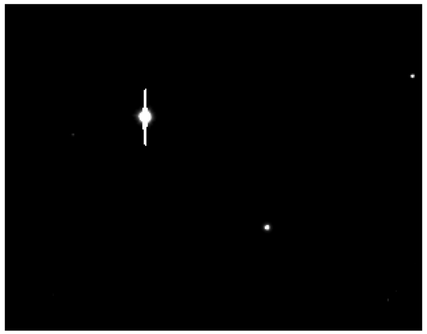

NGC 3783: *linear* intensity scale

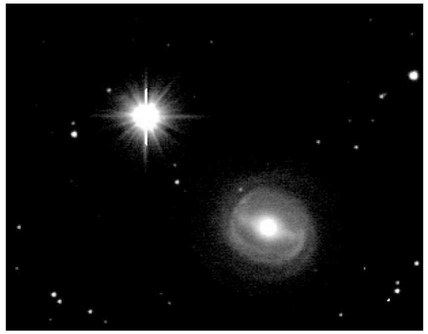

logarithmic intensity scale

Active Galactic Nuclei (AGN): Galaxies with centers as bright as a whole galaxy

NGC 1068 (M77)
(Nordic Optical Telescope)

1908: E. Fath

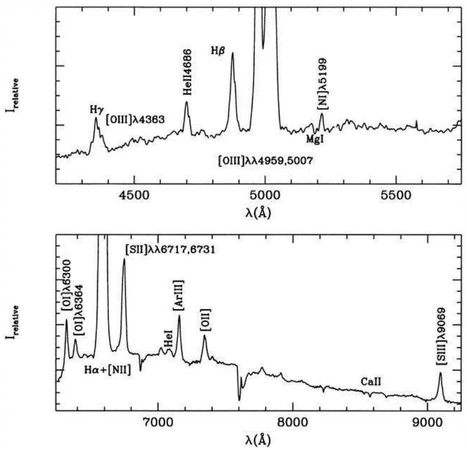

Optical spectrum of NGC 1068

(García-Lorenzo et al., 1999, Fig. 4)

1908: Edward A. Fath: Emission lines in NGC 1068 are similar to those seen in planetary nebulae.

Part of his dissertation!

Differences: very high degree of ionization, large line widths

1918: H. Curtis

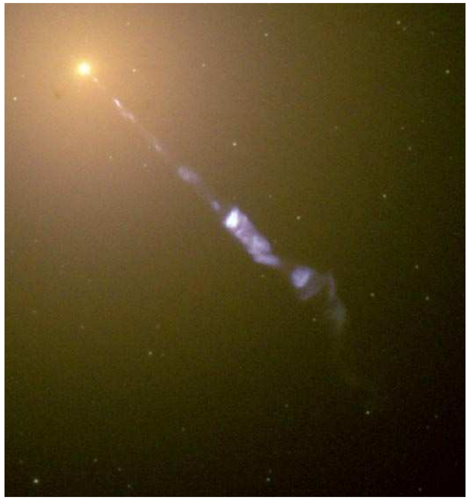

HST

1918: Heber D. Curtis: “[M87 exhibits] a curious straight ray. . . apparently connected with the nucleus by a thin line of matter”.

$\Longrightarrow$ M87 contains an optical jet

1943: C. Seyfert

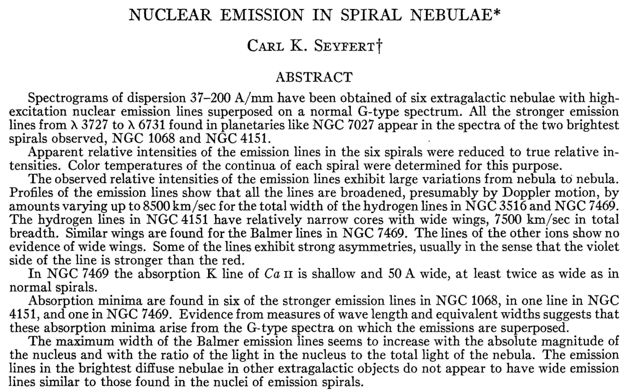

NUCLEAR EMISSION IN SPIRAL NEBULAE*

CARL K. SEYFERT†

ABSTRACT

Spectrograms of dispersion 37–200 A/mm have been obtained of six extragalactic nebulae with high-excitation nuclear emission lines superposed on a normal G-type spectrum. All the stronger emission lines from λ 3727 to λ 6731 found in planetaries like NGC 7027 appear in the spectra of the two brightest spirals observed, NGC 1068 and NGC 4151.

Apparent relative intensities of the emission lines in the six spirals were reduced to true relative intensities. Color temperatures of the continua of each spiral were determined for this purpose.

The observed relative intensities of the emission lines exhibit large variations from nebula to nebula. Profiles of the emission lines show that all the lines are broadened, presumably by Doppler motion, by amounts varying up to 8500 km/sec for the total width of the hydrogen lines in NGC 3516 and NGC 7469. The hydrogen lines in NGC 4151 have relatively narrow cores with wide wings, 7500 km/sec in total breadth. Similar wings are found for the Balmer lines in NGC 7469. The lines of the other ions show no evidence of wide wings. Some of the lines exhibit strong asymmetries, usually in the sense that the violet side of the line is stronger than the red.

In NGC 7469 the absorption K line of *Ca* II is shallow and 50 A wide, at least twice as wide as in normal spirals.

Absorption minima are found in six of the stronger emission lines in NGC 1068, in one line in NGC 4151, and one in NGC 7469. Evidence from measures of wave length and equivalent widths suggests that these absorption minima arise from the G-type spectra on which the emissions are superposed.

The maximum width of the Balmer emission lines seems to increase with the absolute magnitude of the nucleus and with the ratio of the light in the nucleus to the total light of the nebula. The emission lines in the brightest diffuse nebulae in other extragalactic objects do not appear to have wide emission lines similar to those found in the nuclei of emission spirals.

(Seyfert, 1943)

1943: Carl Seyfert: There is a class of spiral galaxies with optical *emission lines*

$\Longrightarrow$ Seyfert Galaxies

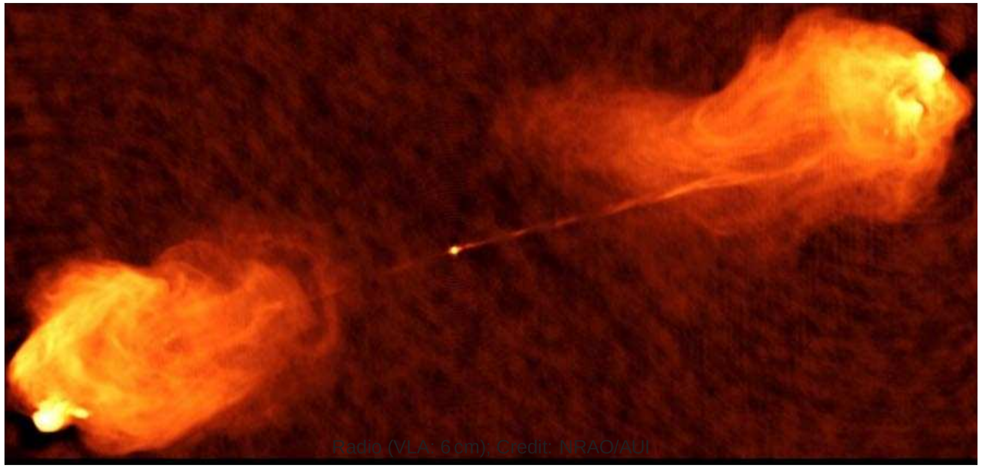

The powerful radio galaxy Cygnus A

1954: W. Baade and R. Minkowski

W. Baade (Mt. Wilson Obs.)

IDENTIFICATION OF THE RADIO SOURCES IN CASSIOPEIA, CYGNUS A, AND PUPPIS A

W. Baade and R. Minkowski
Mount Wilson and Palomar Observatories
Carnegie Institution of Washington
California Institute of Technology

Received June 19, 1953

ABSTRACT

The radio sources in Cassiopeia and Puppis A are identified with a new type of galactic emission nebulosity. The outstanding features of these nebulosities are very large internal random velocities. The radio source Cygnus A is an extragalactic object, two galaxies in actual collision.

Only very few individual sources of cosmic radio emission have been identified with conspicuous astronomical objects.[1] Although the sources in Cassiopeia[2] and Cygnus A[3]

(Baade & Minkowski, 1954)

1954: Walter Baade and Rudolph Minkowski: Bright radio sources have galaxies as optical counterparts

Cyg A: 2nd brightest radio source on the sky.

1959: L. Woltjer

EMISSION NUCLEI IN GALAXIES

L. Woltjer*
Yerkes Observatory, University of Chicago

Received February 16, 1959

ABSTRACT

Some galaxies which show wide emission lines in the spectra of their nuclei are discussed. It is shown that, on statistical grounds, the nuclear emission must last for several times 10^8 years at least. The nuclei are extremely narrow, of the order of 100 parsecs, and, if a normal mass-to-light ratio applies, extremely massive. The width of the emission lines, which indicates velocities of a few thousand kilometers per second, is probably due to fast motions, circular or random, in the gravitational fields of the nuclei. The high star density in the nuclei may provide a source of excitation. In the nucleus of our own Galaxy the radio source Sagittarius gives evidence of strong magnetic fields and large amounts of relativistic particles. A mass of a few times 10^8 solar masses is needed to prevent disintegration of the source. The Andromeda Nebula has a nucleus with a somewhat smaller mass. The occurrence of dense nuclei may be a common characteristic of many galaxies.

(Woltjer, 1959)

1959: Lodewijk Woltjer: Objects must have very large masses.

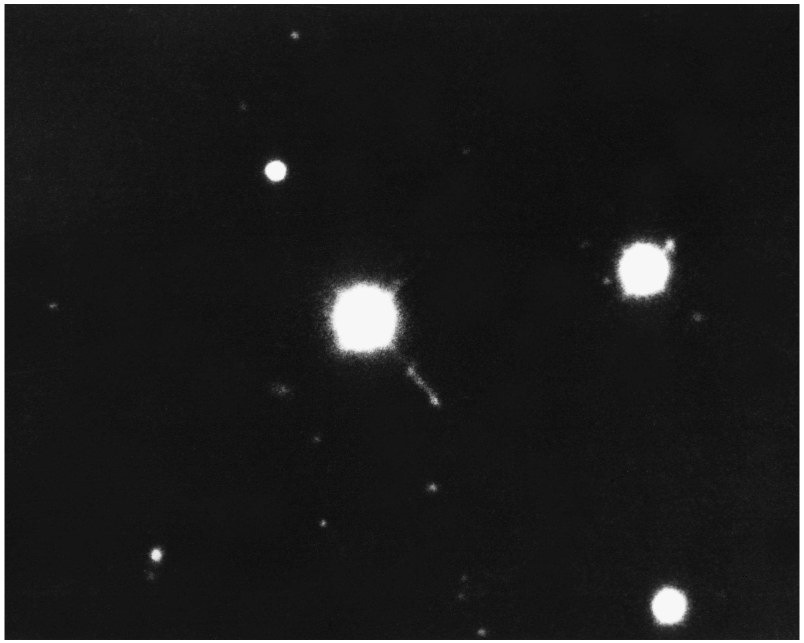

3C273 (4 m Myall telescope, NOAO/AURA/NSF)

1963: M. Schmidt

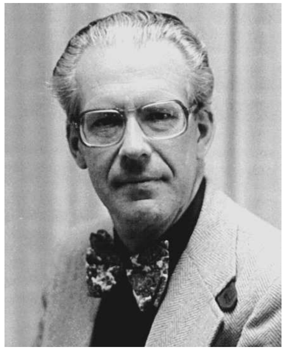

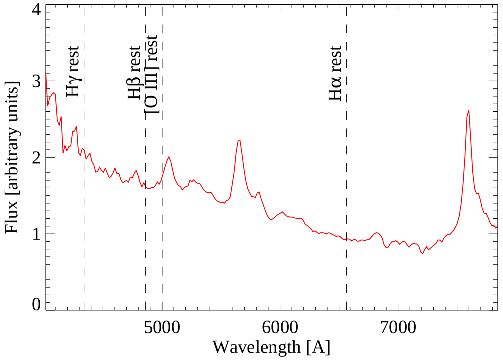

M. Schmidt (Caltech)

3C273 (Rondi et al., Pic du Midi)

1963: Maarten Schmidt: 3C273

1963: M. Schmidt

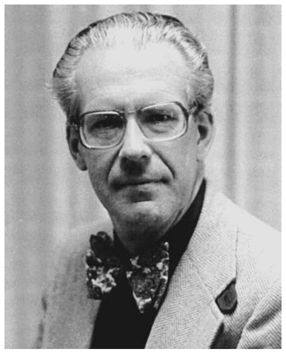

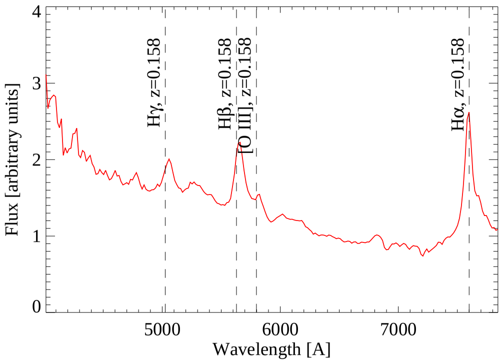

M. Schmidt (Caltech)

3C273 (Rondi et al., Pic du Midi)

1963: Maarten Schmidt: 3C273 has $z = 0.158 \Longrightarrow$ objects are far away!

$z = 0.158$ corresponds to $d = 1.74$ Gpc (3 billion ly)

shortly after this: 1963: J. Greenstein and Th. Matthews: 3C48 has $z = 0.368$

Seyfert Galaxies, I

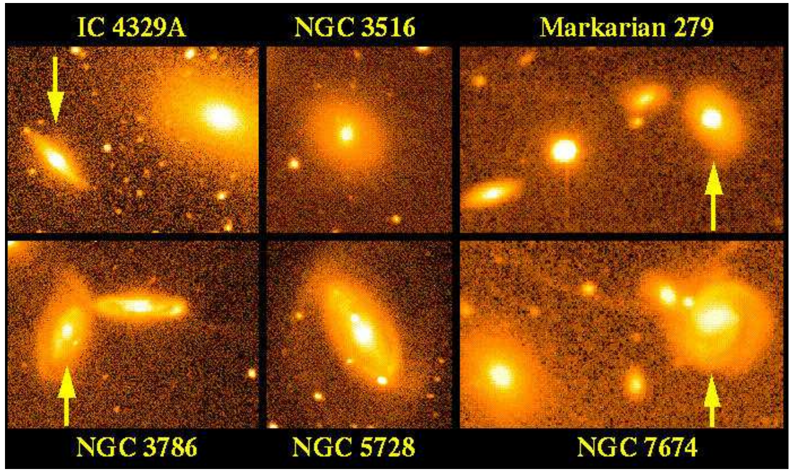

W. Keel

Seyfert Galaxies: point-like sources in the centers of galaxies, normally galaxy is detectable; two types: Seyfert 1 galaxies and Seyfert 2 galaxies.

Seyfert Galaxies, II

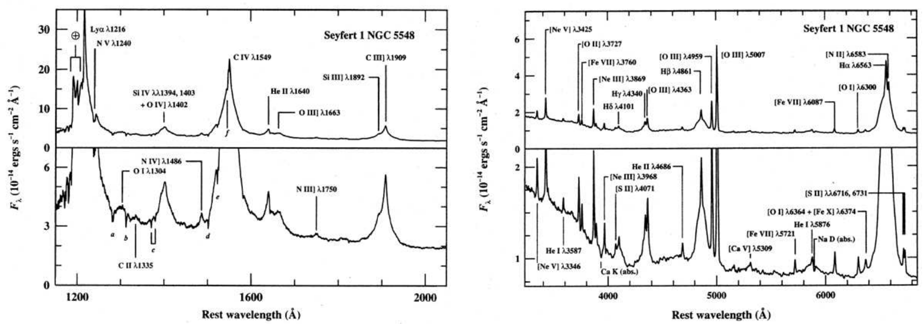

Seyfert 1 galaxies

- broad allowed lines (e.g., from H), with widths corresponding up to 10^4 km s^{-1} from a medium of high density ($n_e \gtrsim 10^9$ cm^{-3}).
- Thin forbidden lines (e.g., [O III5007]), FWHM $\sim$ few $\cdot\, 10^2$ km s^{-1} from a thin medium ($n_e \sim 10^3$ cm^{-3} ... 10^6 cm^{-3}).

Velocity width from Doppler effect: $\Delta\lambda/\lambda = v/c$.

Seyfert 2

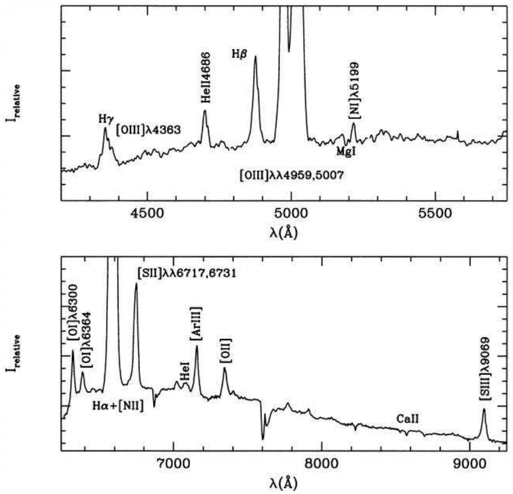

Spectrum of the Seyfert 2 galaxy NGC 1068:

- weak continuum (compared to Seyfert 1s).
- thin forbidden lines, $\sim$ few $\cdot 10^2\,\mathrm{km\,s^{-1}}$.
- no broad lines

(García-Lorenzo et al., 1999, Fig. 4)

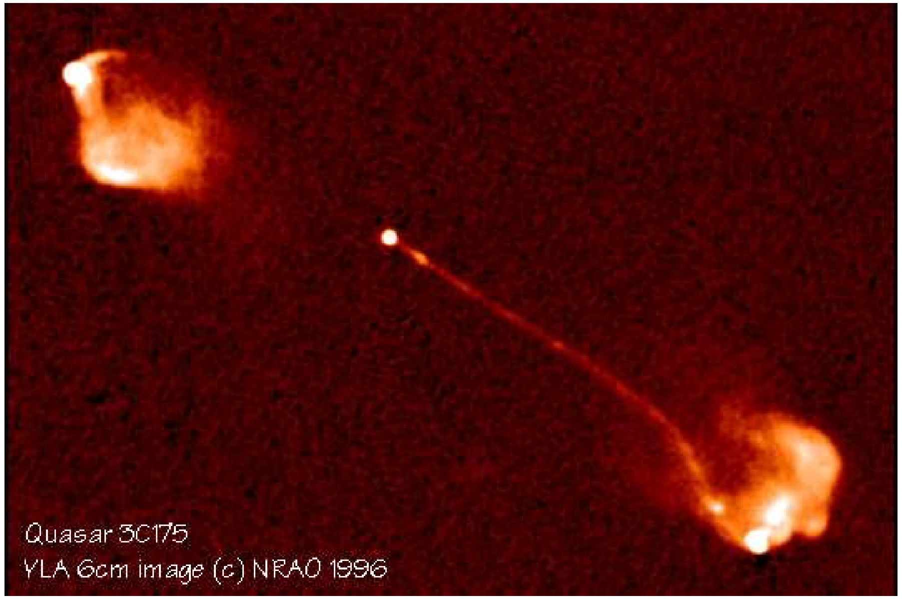

A. Bridle (priv. comm.)

Radio image of 3C175 ($z = 0.768$):
A typical FR 2 Galaxy

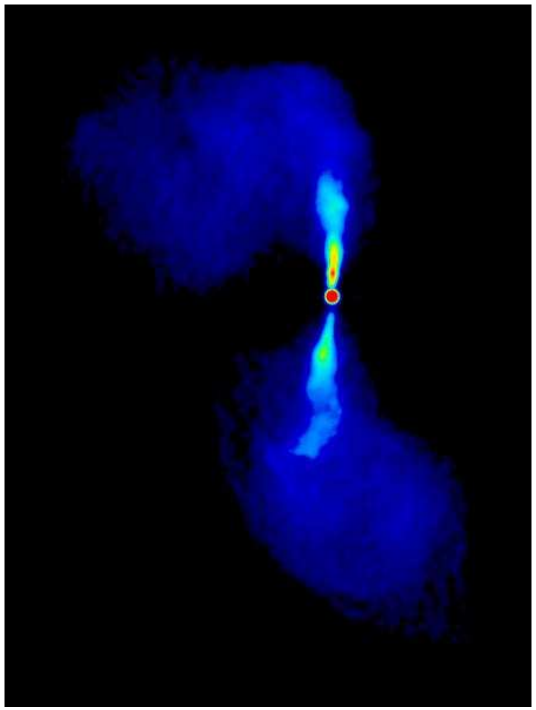

Radio image of M84 (3C272.1):
A typical Fanaroff Riley Type 1 Galaxy

Laing & Bridle (1987); VLA 4885 MHz, $134'' \times 170''$

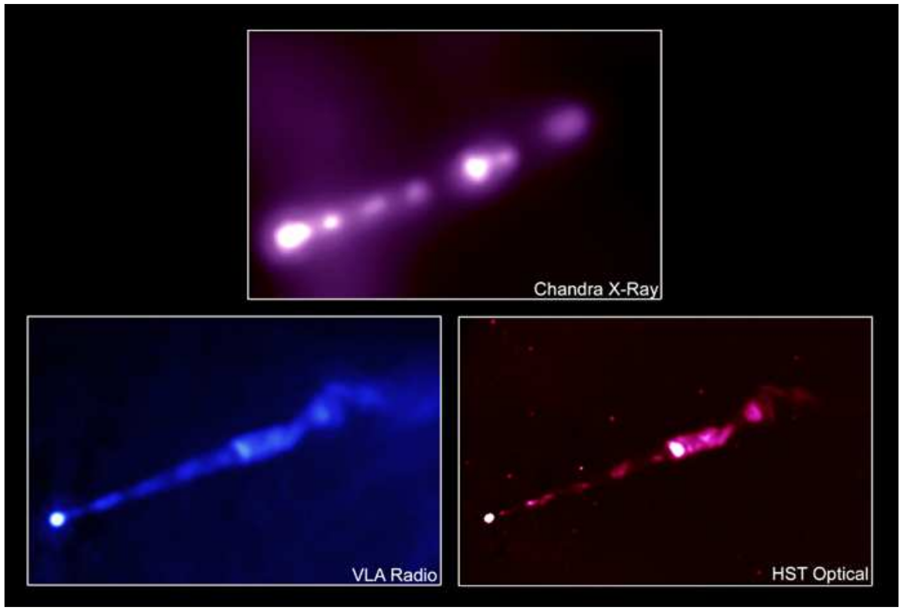

X-ray: NASA/CXC/MIT/H.Marshall et al. Radio: F.Zhou, F.Owen (NRAO), J.Biretta (STScI)
Optical: NASA/STScI/UMBC/E.Perlman et al.

Since the 1960s: multi wavelength astronomy

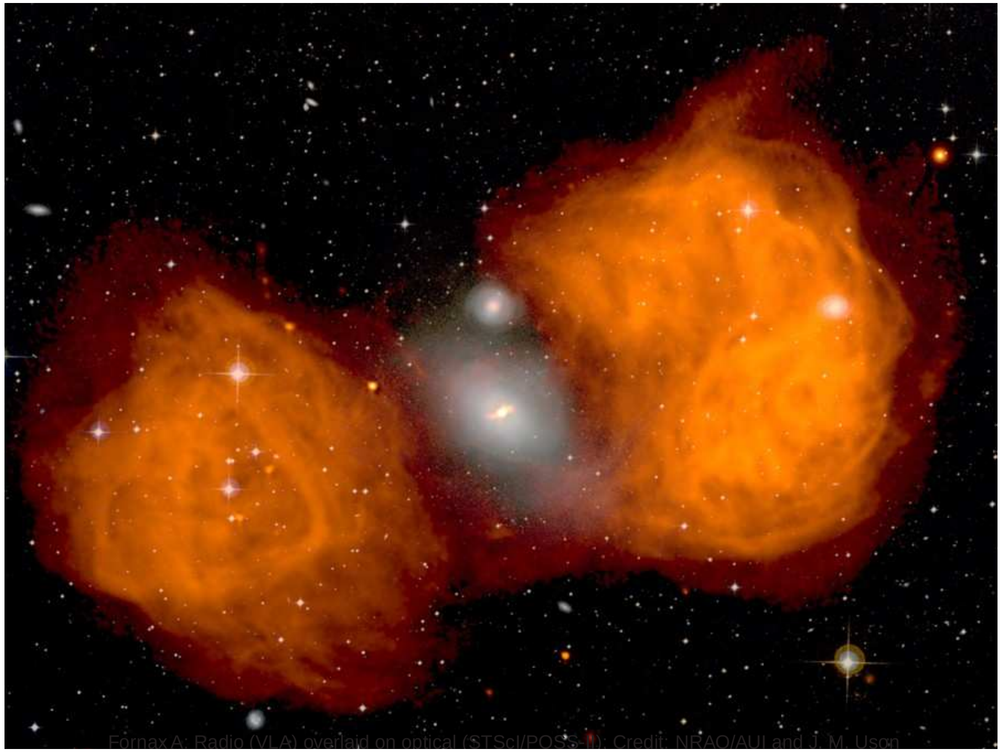

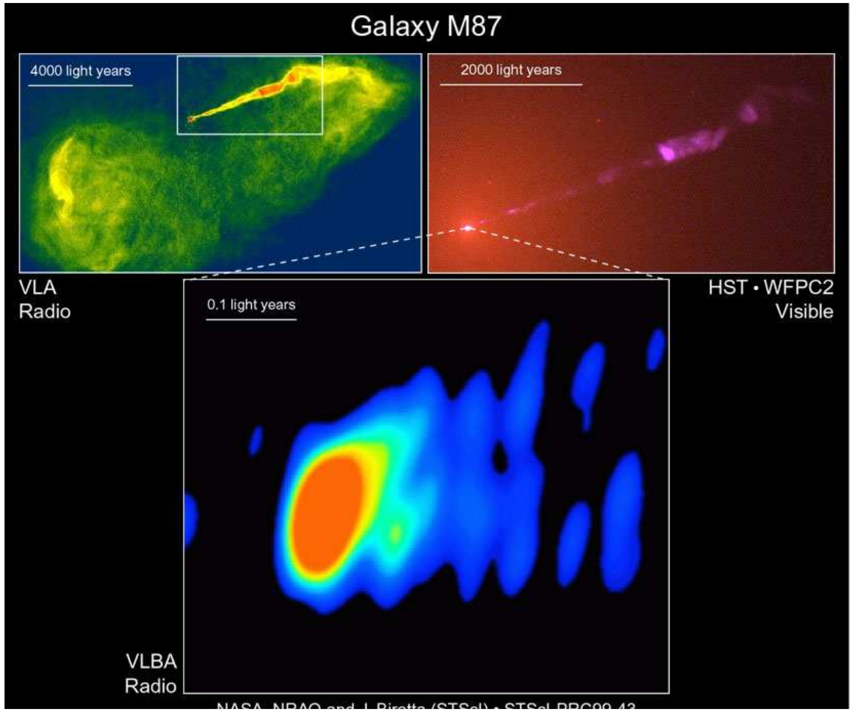

M87 – R. Gendler

http://www.robgendlerastropics.com/M87NM.html

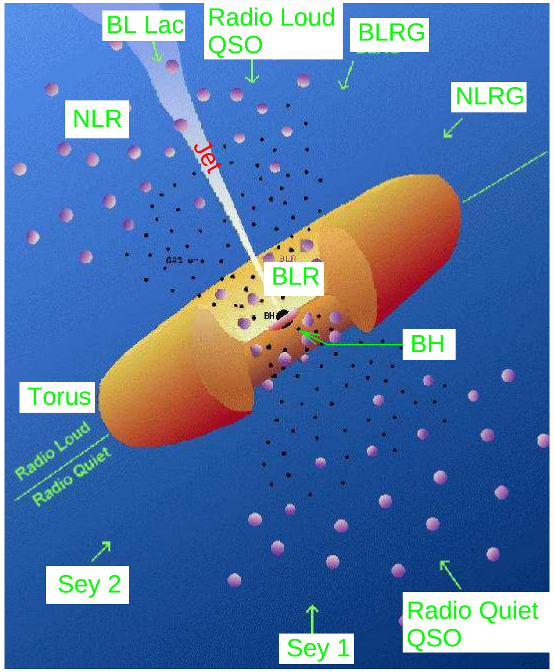

Unification: Assumes physics of all AGN is the same, phenomenology is due to different lines of sight.

(Urry & Padovani, 1995, Important: length scale is not linear!)

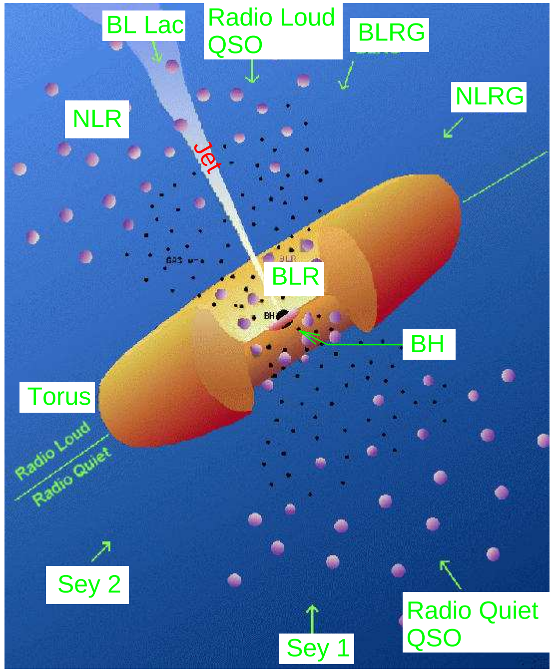

Physical properties:

Accretion disc: $r \sim 10^{-3}$ pc,
- $n \sim 10^{15}\,\mathrm{cm}^{-3}$,
- $kT \sim 50\,\mathrm{eV} \cdot r^{-3/4}$,
- $v \sim 0.3c$ at the inner edge.

Broad Line Region (BLR): $r \sim$ 0.01–0.1 pc (=light days or less),
- $n \sim 10^{10}\,\mathrm{cm}^{-3}$,
- $v \sim 1000$–$5000\,\mathrm{km\,s}^{-1}$,
- $T \sim 10^4\,\mathrm{K}$

Torus: $r \sim$ 1– few 10 pc,
- $n \sim 10^3$–$10^6\,\mathrm{cm}^{-3}$,
- T: cold

Narrow Line Region (NLR):
- $r \sim$ 100–1000 pc,
- $n \sim 10^3$–$10^6\,\mathrm{cm}^{-3}$,
- $v \sim$ few100 $\mathrm{km\,s}^{-1}$,
- $T \sim 10^4\,\mathrm{K}$

X-Ray Spectra, I

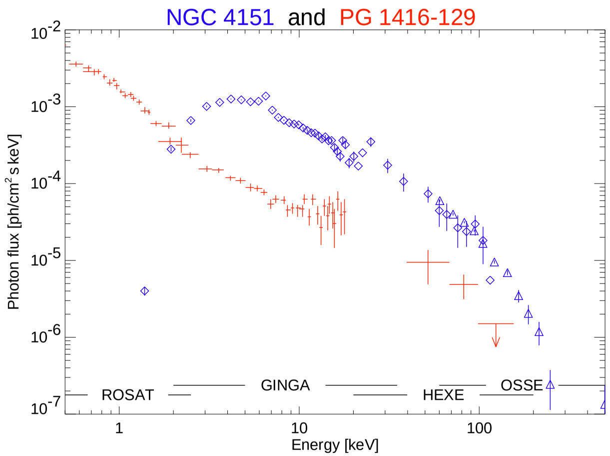

(PG 1416−129: de Kool et al., 1994, Williams et al., 1992, Staubert & Maisack, 1996; NGC 4151: Maisack 1991, 1993)

Note: NGC 4151 not corrected for interstellar absorption.

X-Ray Spectra, II

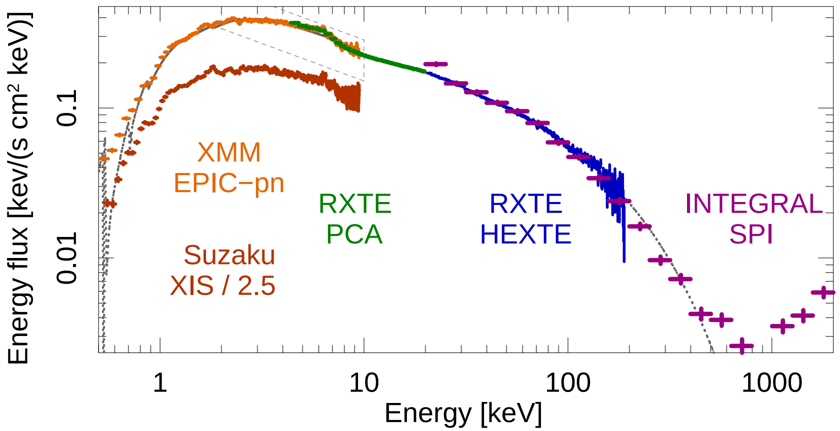

Cyg X-1 (Hanke, et al., 2008)

Spectral shape of Seyferts is very similar to Galactic Black Holes $\Longrightarrow$
Same physical mechanism (=Comptonization) responsible!

Comptonization, I

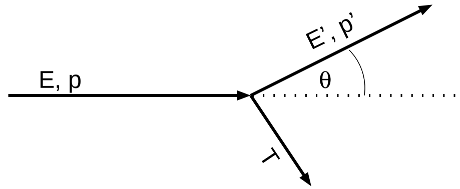

Thomson scattering: initial and final wavelength are identical.
But: in reality: light consists of photons
$\Longrightarrow$ Scattering: photon changes direction
$\Longrightarrow$ Momentum change
$\Longrightarrow$ Energy change!
This is a quantum picture
$\Longrightarrow$ Compton scattering.

Dynamics of scattering gives energy/wavelength change:

$$E' = \frac{E}{1 + \frac{E}{m_e c^2}(1 - \cos\theta)} \quad \text{or} \quad \lambda' - \lambda = \frac{h}{m_e c}(1 - \cos\theta) \tag{5.1}$$

Averaging over θ, for $E \ll m_e c^2$:

$$\frac{\Delta E}{E} \approx -\frac{E}{m_e c^2} \tag{5.2}$$

For thermal photons: energy transfer onto electron possible:

$$\frac{\Delta E}{E} = \frac{4kT - E}{m_e c^2} \tag{5.3}$$

Comptonization, II

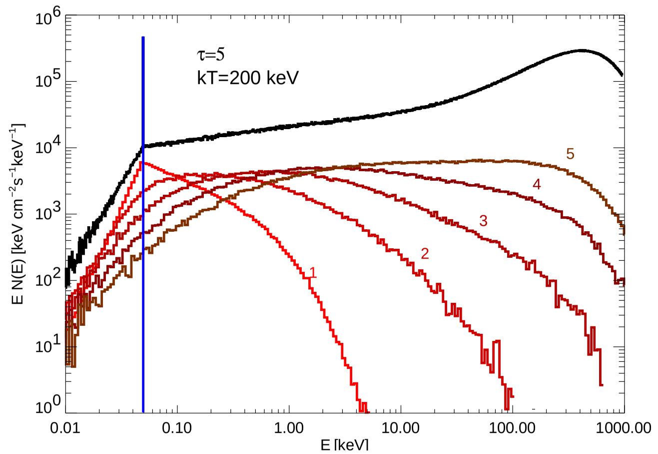

Monte Carlo simulation shows: Spectrum is $\Longrightarrow$ Power law with exponential cut-off (here: with additional “Wien hump”).

Comptonization, III

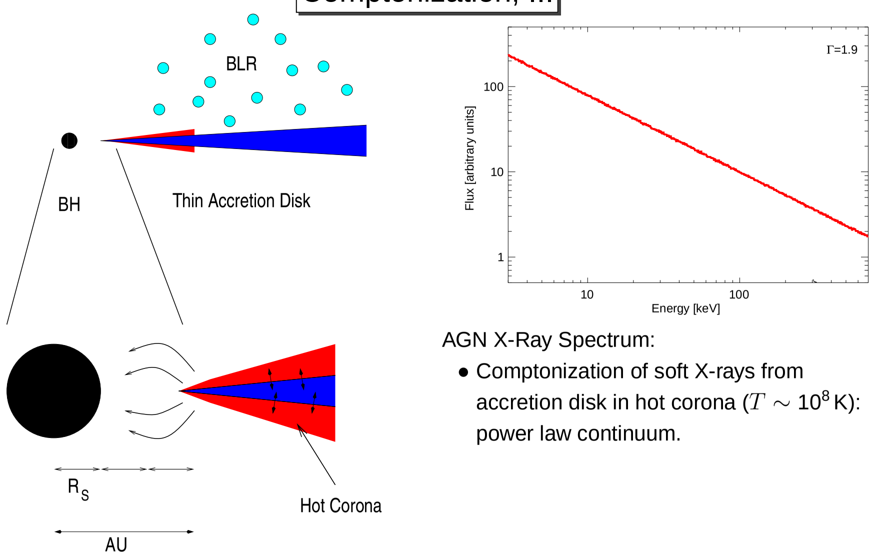

AGN X-Ray Spectrum:

- Comptonization of soft X-rays from accretion disk in hot corona ($T \sim 10^8$ K): power law continuum.

Comptonization, IV

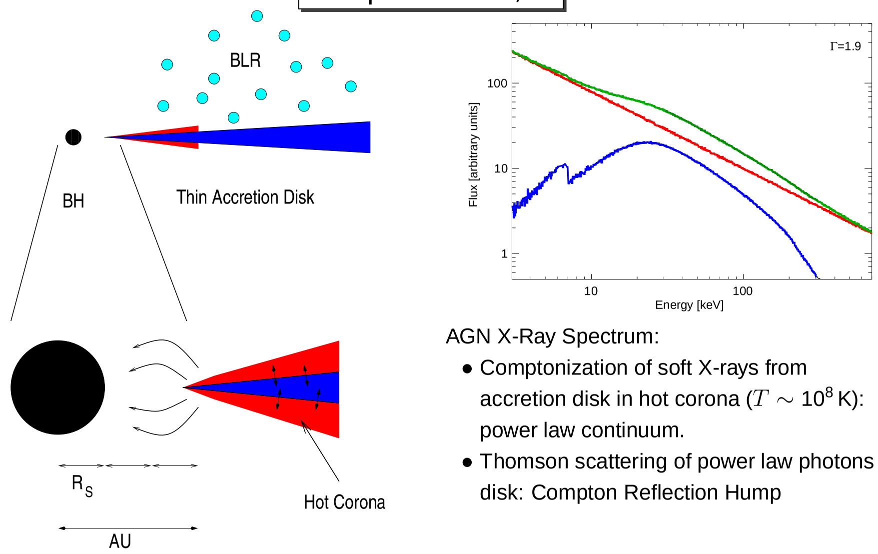

AGN X-Ray Spectrum:

- Comptonization of soft X-rays from accretion disk in hot corona ($T \sim 10^8$ K): power law continuum.
- Thomson scattering of power law photons in disk: Compton Reflection Hump

Comptonization, V

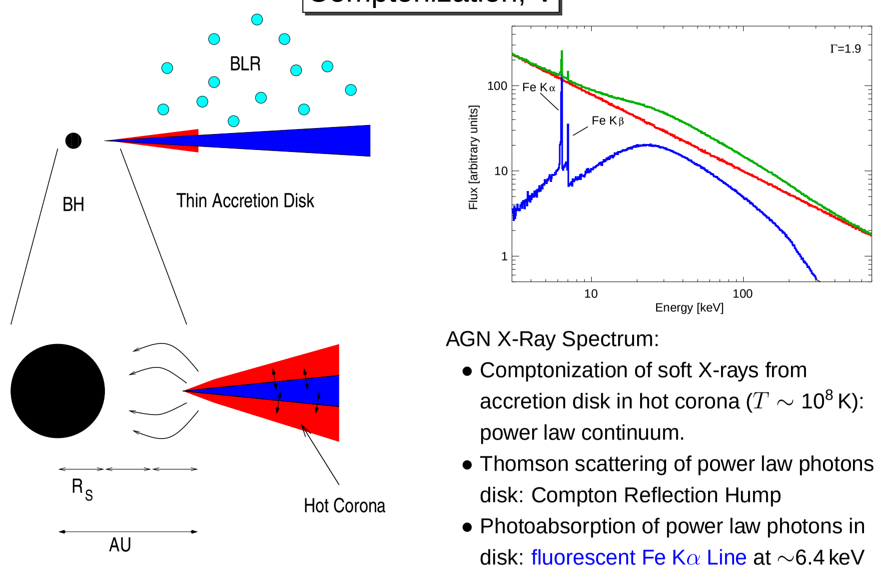

AGN X-Ray Spectrum:

- Comptonization of soft X-rays from accretion disk in hot corona ($T \sim 10^8$ K): power law continuum.
- Thomson scattering of power law photons in disk: Compton Reflection Hump
- Photoabsorption of power law photons in disk: fluorescent Fe Kα Line at $\sim$6.4 keV

Seyfert X-Ray Spectra, I

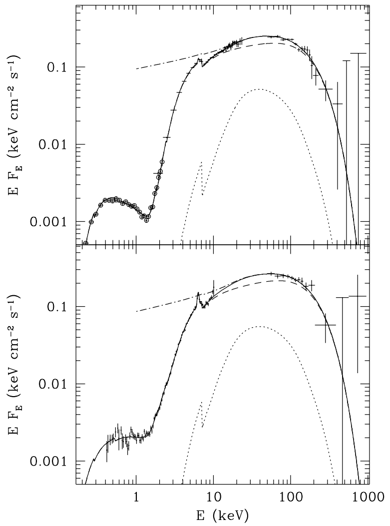

Comptonization explains broad-band Seyfert spectra very well

Example: Fits of Comptonization models to broad-band spectrum of Seyfert 1 galaxy NGC 4151 showing all three components:

- $kT_e \sim 88^{+55}_{-26}$ keV
- $N_H \sim 7 \times 10^{22}$ cm^{-2} and 13×10^{22} cm^{-2}, respectively
- Reflection factor: $\Omega/2\pi = 0.43$ (assumed; consistent with Fe line, but not significantly detected in these data [but in other AGN]).

Note strong absorption present in Seyfert 1 X-ray spectra!

(Zdziarski et al., 1996)

Seyfert X-Ray Spectra, II

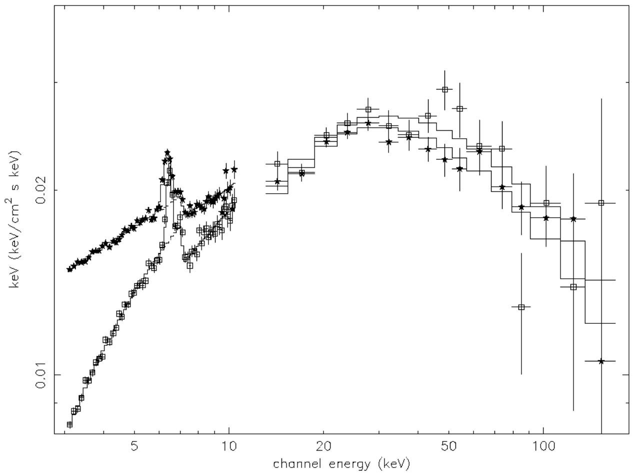

(Average Sy 1 and Sy 2 spectra from *BeppoSAX*; **?**, Fig. 4)

Spectra of Sy 1 and Sy 2 are very similar, except for lower N_H in Sy 2

Variability, I

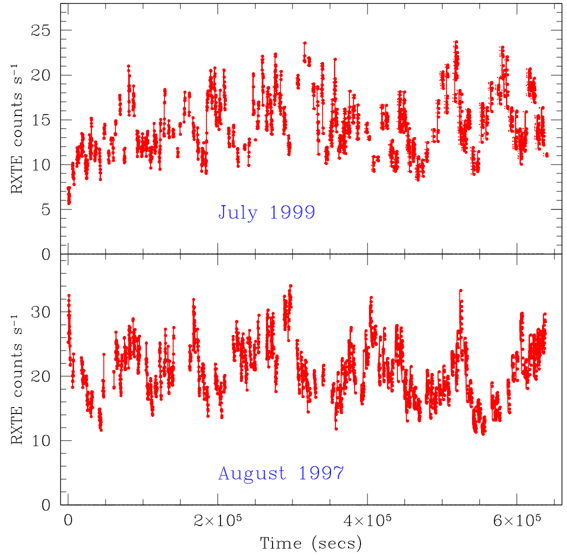

AGN are strongly variable

Timescale at $r_{ISCO} = 6GM/c^2$:

$$t \sim \frac{2\pi r_{ISCO}}{\sqrt{GM/r_{ISCO}}} \propto \frac{r^{3/2}}{M^{1/2}} \propto M \qquad (5.4)$$

so less variable for higher BH mass.

(MGC−6-30-15; McHardy et al., 2005)

Variability, II

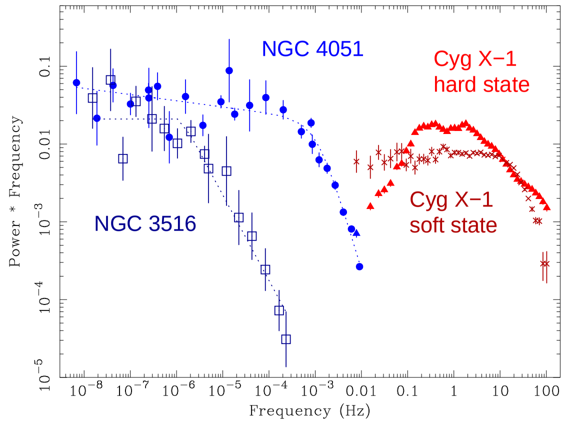

(NGC 4051; McHardy et al., 2004)

Seyfert power spectra (=squared Fourier transform) are similar to galactic black hole power spectra in the soft state.

Variability, III

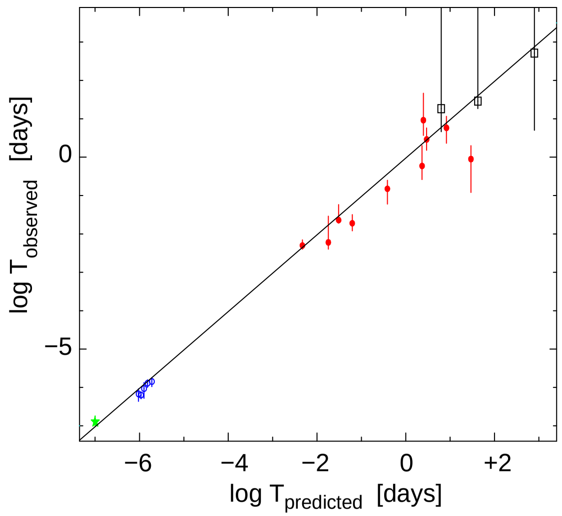

McHardy et al. (2006): Timescale of PSD break scales as

$$\log T_{\text{break}} = (2.10 \pm 0.15) \log M_{\text{BH}} - (0.98 \pm 0.15) \log L_{\text{bol}} - (2.32 \pm 0.20)$$

Since $L_{\text{bol}} \sim \dot{m}_{\text{Edd}} \dot{L}_{\text{Edd}}$ where $\dot{m}_{\text{Edd}} = \dot{M}/\dot{M}_{\text{Edd}}$:

$$T_{\text{break}} \propto M_{\text{BH}}^{1.12} \dot{m}_{\text{Edd}}^{-0.98}$$

(McHardy et al., 2006)

Relativistic Lines and BH Paradigm, I

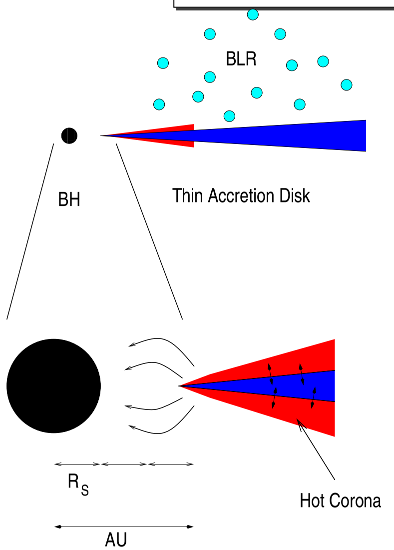

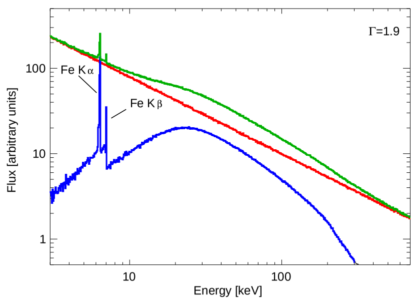

AGN X-Ray Spectrum:

- Comptonization of soft X-rays from accretion disk in hot corona ($T \sim 10^8$ K): power law continuum.
- Thomson scattering of power law photons in disk: Compton Reflection Hump
- Photoabsorption of power law photons in disk: fluorescent Fe Kα Line at ~6.4 keV

Relativistic Lines and BH Paradigm, II

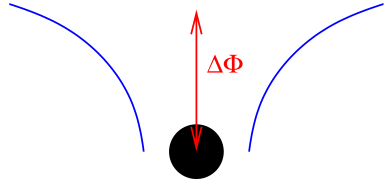

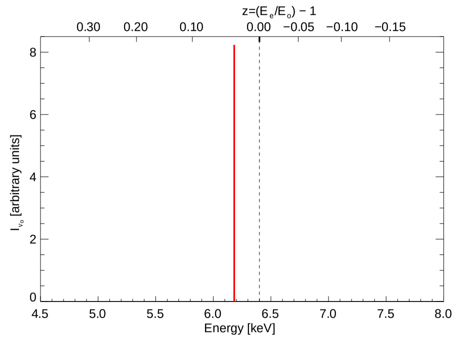

Total observed line profile affected by

- grav. Redshift

Relativistic Lines and BH Paradigm, III

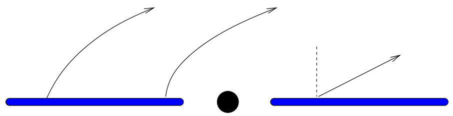

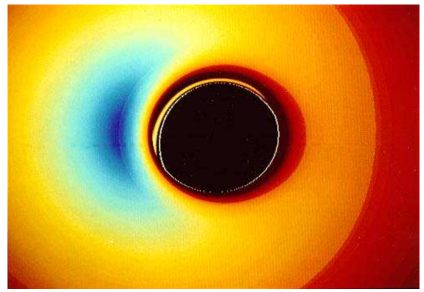

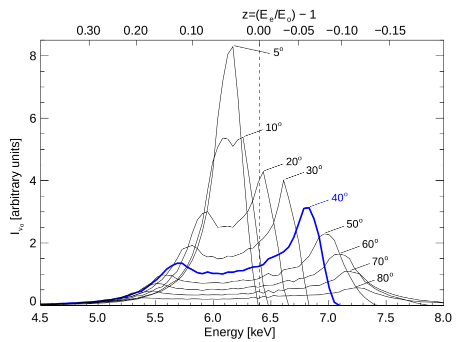

Total observed line profile affected by

- grav. Redshift
- Light bending
- rel. Doppler shift

Relativistic Lines and BH Paradigm, IV

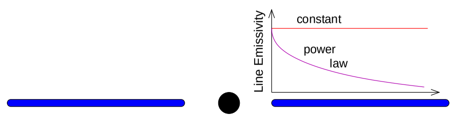

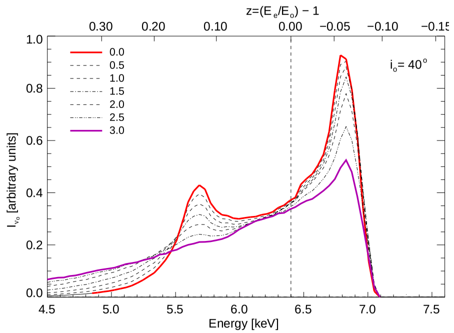

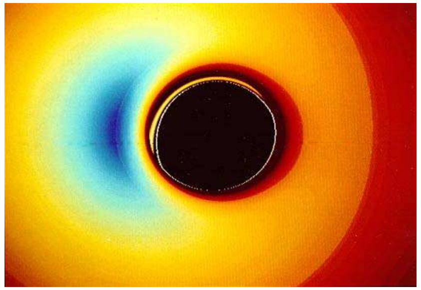

Total observed line profile affected by

- grav. Redshift
- Light bending
- rel. Doppler shift
- emissivity profile

Relativistic Lines and BH Paradigm, V

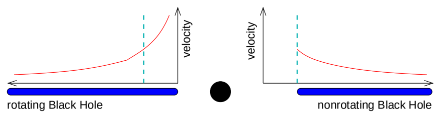

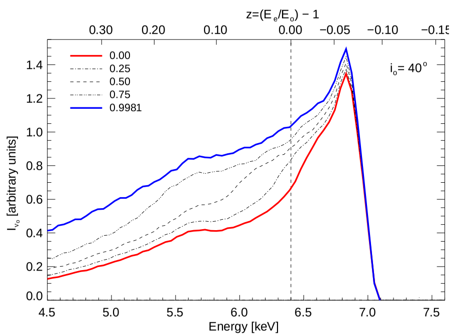

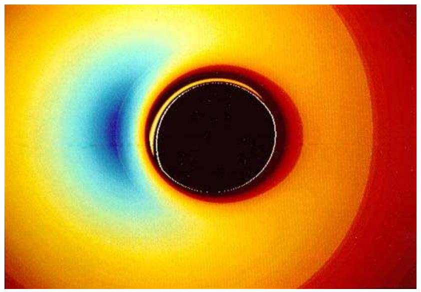

Total observed line profile affected by

- grav. Redshift
- Light bending
- rel. Doppler shift
- emissivity profile
- spin of black hole

ASCA: MCG−6-30-15, I

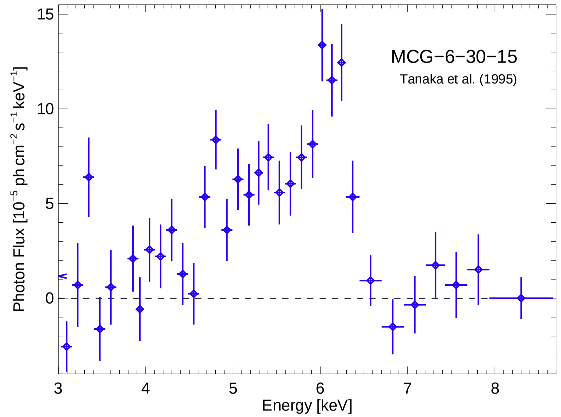

Tanaka et al. (1995): time averaged *ASCA* spectrum of Seyfert 1 MCG−6-30-15: line skew symmetric

⟹ Schwarzschild black hole.

ASCA: MCG−6-30-15, II

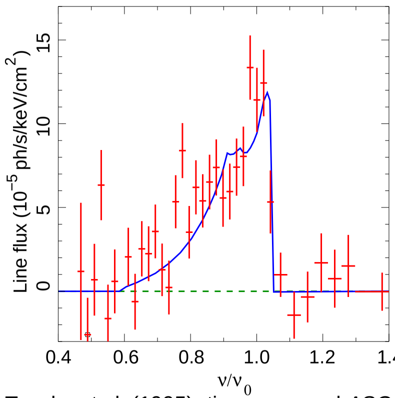

Tanaka et al. (1995): time averaged *ASCA* spectrum: line skew symmetric

⟹ Schwarzschild black hole.

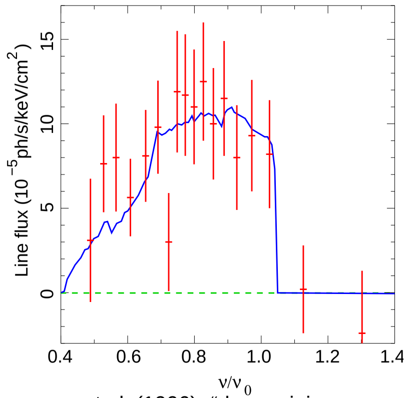

Iwasawa et al. (1996): “deep minimum state”: extremely broad line

⟹ Kerr Black Hole.

Later confirmed with *BeppoSAX* (Guainazzi et al., 1999) and *RXTE* (Lee et al., 1999).

XMM: MCG−6-30-15, I

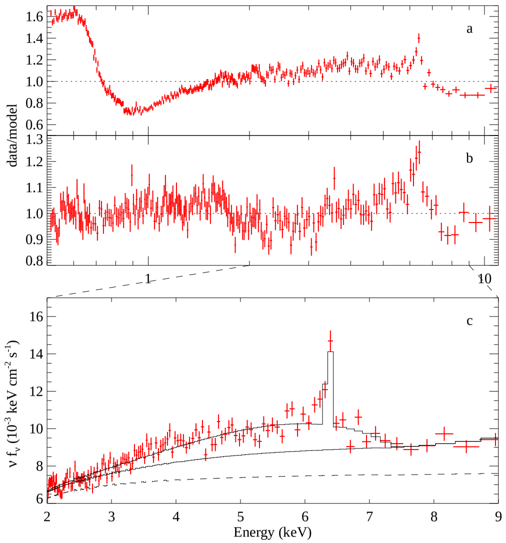

pure PL fit

Better modeling of soft excess and reflection $\Longrightarrow$ Fe Kα line has extreme width and skewed profile.

Components of the final fit.
$\Longrightarrow$ Line emissivity is strongly concentrated towards the inner edge of the disk ($\epsilon \propto r^{-4.6}$; cannot be explained with standard α-disk)

(*XMM-Newton*, June 2000, 100 ksec; Wilms et al., 2001)

XMM: MCG−6-30-15, II

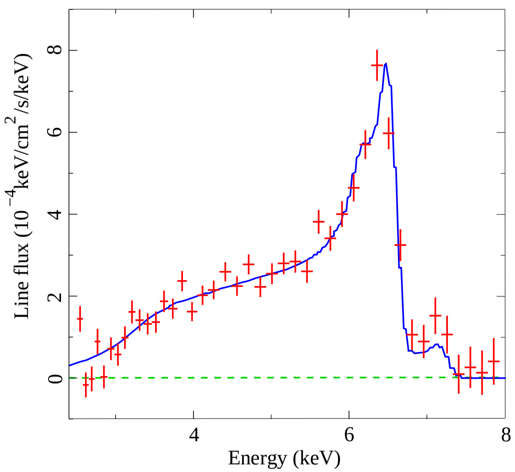

Fabian et al. (2002)

2001 July/August: 315 ksec observation (Fabian et al., 2002)

- Strong narrow line
- broad line clearly present
- emissivity profile very steep for radii close to $r_{\rm in}$

$I_{\text{Fe K}\alpha} \propto r^{-5.5\pm0.3}$ for $r < 6.1^{+0.8}_{-0.5} r_{\rm g}$, $\propto r^{-2.7\pm0.1}$ outside that;
Fabian & Vaughan (2003); confirms Wilms et al. (2001)

XMM: MCG−6-30-15, III

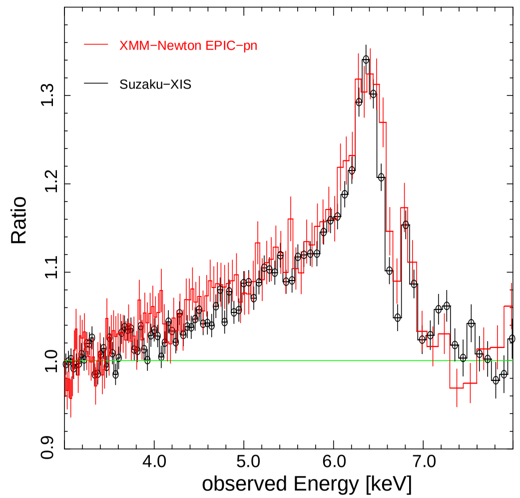

Suzaku (2006 Jan; ~350 ksec; Miniutti et al., 2007)

Brenneman & Reynolds (2006): Angular momentum of BH in MGC−6-30-15: $a = 0.989^{+0.009}_{-0.002}$.

Assuming no emission from inside the inner-most stable circular orbit, strongly constrained geometry.

Other Sources

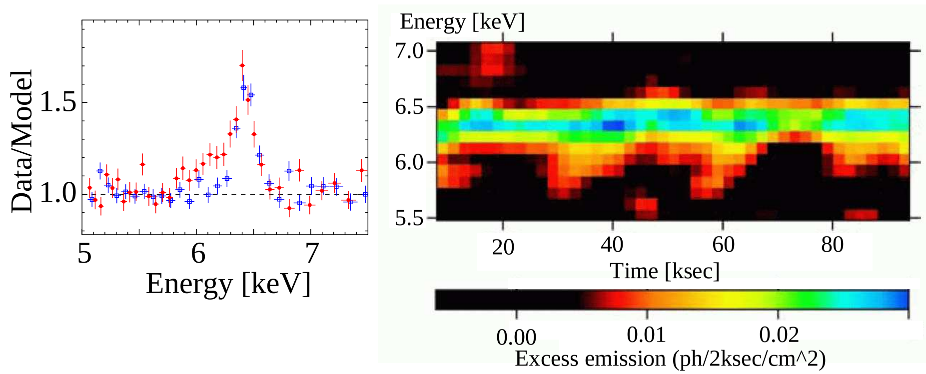

(Iwasawa et al., 2004, Figs. 3,4)

Line profile variability in NGC 3516 $\Longrightarrow$ Corotating flare? ($7r_{\rm g} \lesssim r \lesssim 16 r_{\rm g}$)

If interpretation is pushed further, gives $M \sim (1 \ldots 5) \times 10^7 M_\odot$.

Other Sources

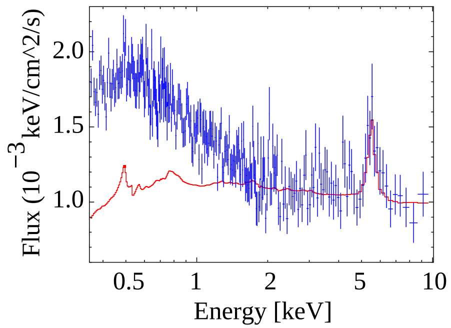

(Porquet & Reeves, 2003, Fig. 3)

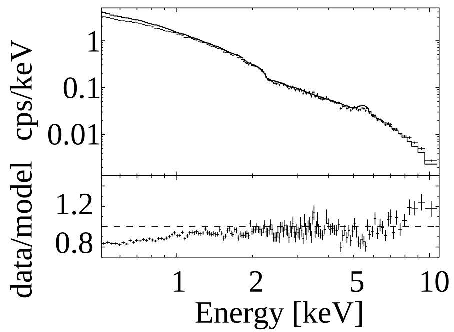

(Matt et al., 2005, Fig. 1)

XMM data from 2001

comparison 2003 vs. 2001 data

Q0056−363 (broad line radio-quiet quasar, $L_X > 10^{45}\,\mathrm{erg\,s^{-1}}$):

Fe Kα has FWHM $24500\,\mathrm{km\,s^{-1}}$, EW 275 eV

Q0056−363 is highest luminosity RQ-QSO with broad Fe Kα line.

Other Sources

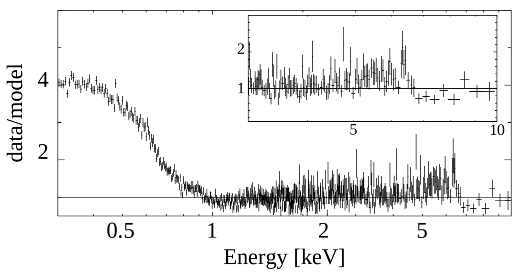

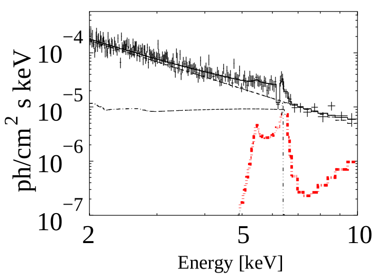

(Longinotti et al., 2003)

IRAS 13349+2436:

- Model either 2 broad emission lines *or*
- relativistic line from Fe XXIII/XXIV plus narrow absorption feature

Line shape can be rather complex!

Other examples include *blue*shifted lines, e.g., in Mkn 205 (Reeves et al., 2001) or Mkn 766.

Absorption or Lines?

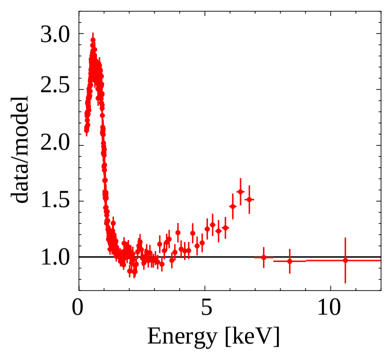

(1H0707−495; Fabian et al., 2004)

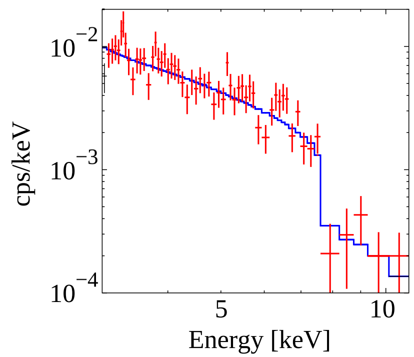

(IRAS 13224−3809; Boller et al., 2003)

Narrow Line Sy1: Strong absorption or a relativistic line fron a reflection dominated spectrum both describe the data equally well!

Similar results have been found by Pounds et al. in a variety of sources. . .

But: strong absorption models contradict observations where data >10 keV available.

Narrow Lines

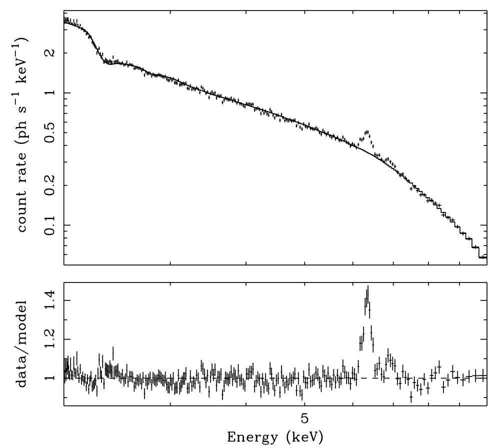

(NGC 4258; Reynolds et al. 2004)

The majority of Seyfert galaxies and QSOs do *not* show evidence for broad Fe Kα lines!

Narrow Lines

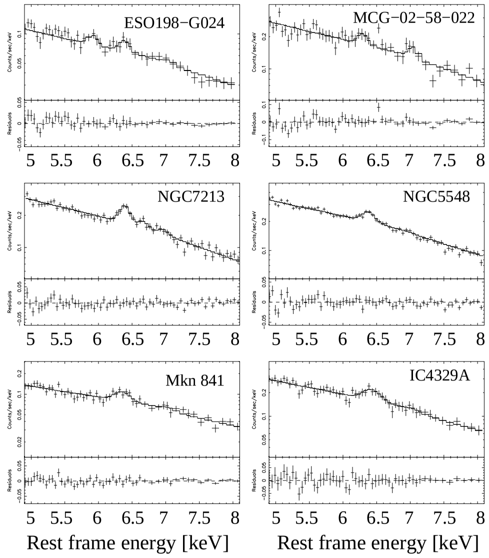

The majority of Seyfert galaxies and QSOs do *not* show evidence for broad Fe Kα lines!

Statistics for PG-QSO: 20/38 show Fe Kα line, of these 3 have broad line (Jiménez-Bailón et al., 2005)

Bianchi et al. (2004, Fig. 4)
[Sample of Seyferts with simultaneous *BeppoSAX* observations.]

Classification, I

At arcsec resolution, most radio-loud AGN are unresolved! But great variety in spectral shape.

Condon et al. (1998); Kuehr et al. (1981)

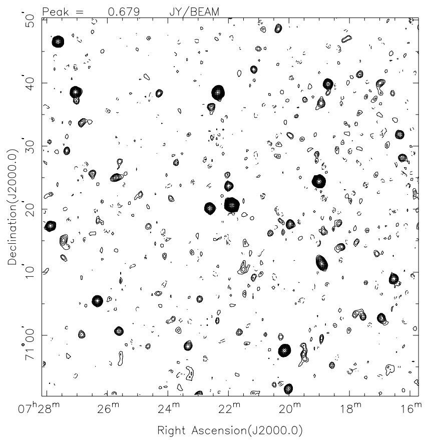

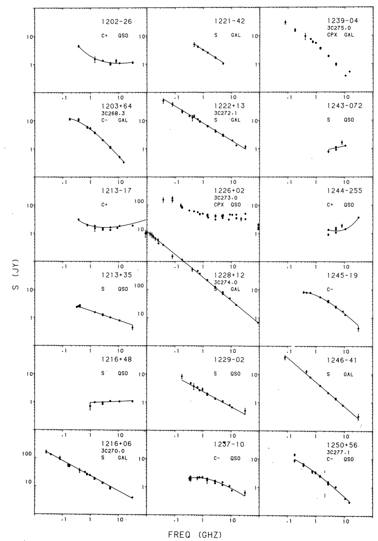

Classification, II

Radio-loud AGN are observed to have strong polarization and power law radio spectra. These are characteristics of synchrotron radiation.

Synchrotron-Radiation (=Magnetobremsstrahlung): Radiation emitted by relativistic electrons in a magnetic field.

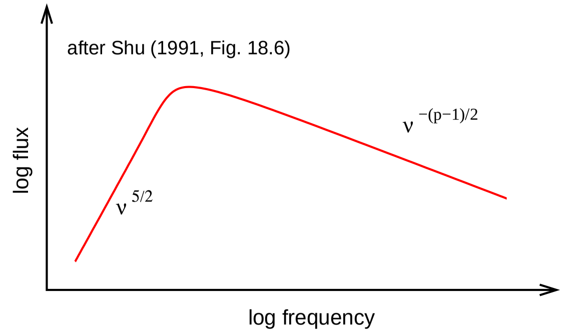

Spectrum of a single synchrotron-emitting blob:
At low ν: optically thick.
At high ν: optically thin.

Turnover: $\tau = 1$ surface

$\tau \propto R$ and $\nu(\tau = 1) \propto R^{-1}$

(R: size of the emitting region).

Classification, III

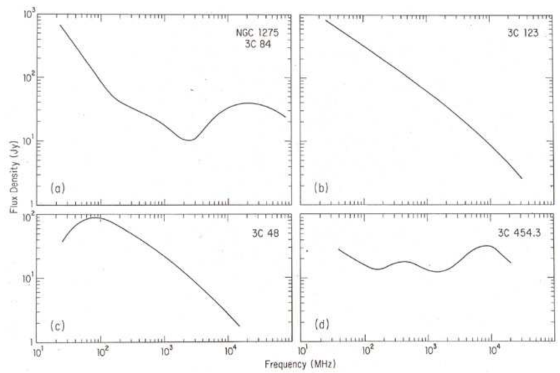

- NGC 1275: extended steep-spectrum emission plus compact self-absorbed nucleus
- 3C123: 3C 123: optically thin at all plotted frequencies
- 3C 48: self-absorbed below 100 MHz
- 3C454.3: superposition of many jet regions which become opaque at different frequencies (flat-spectrum radio quasar)

Classification, IV

Classification of radio-loud AGN is based on morphology and radio spectrum:

1. Powerful double-lobed radio galaxies with hotspots and a steep radio spectrum falling toward higher frequencies (Fanaroff-Riley class II, FR II)
2. Weaker steep-spectrum, double-lobed radio galaxies without leading hotspots (FR I types)
3. Core-dominated flat-spectrum sources (Blazars: quasars and BL Lac objects)
4. Compact steep-spectrum sources (CSS sources) and gigahertz-peaked spectrum sources (GPS sources); no large-scale radio structure; morphological classification term: compact symmetric objects (CSOs) or compact doubles

Observing technique and frequency strongly affects sample (e.g., low-frequency flux-density limited surveys tend to select steep-spectrum sources). Flat-spectrum sources are classical targets for Very-Long-Baseline Interferometry (VLBI) observations, which are sensitive to compact emission.

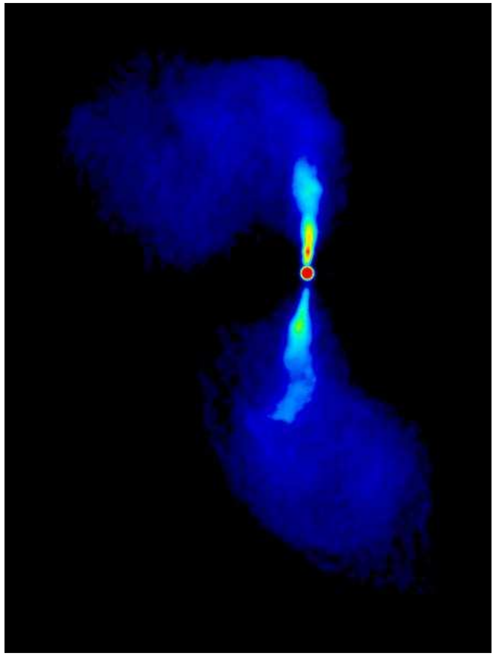

Fanaroff-Riley Type 1: asymmetric jets with wide opening angle ending in plumes

M84 (3C272.1) (Laing & Bridle, 1987):
VLA 4885 MHz, 134″ × 170″; see also
www.jb.man.ac.uk/atlas/other/3C272P1.html

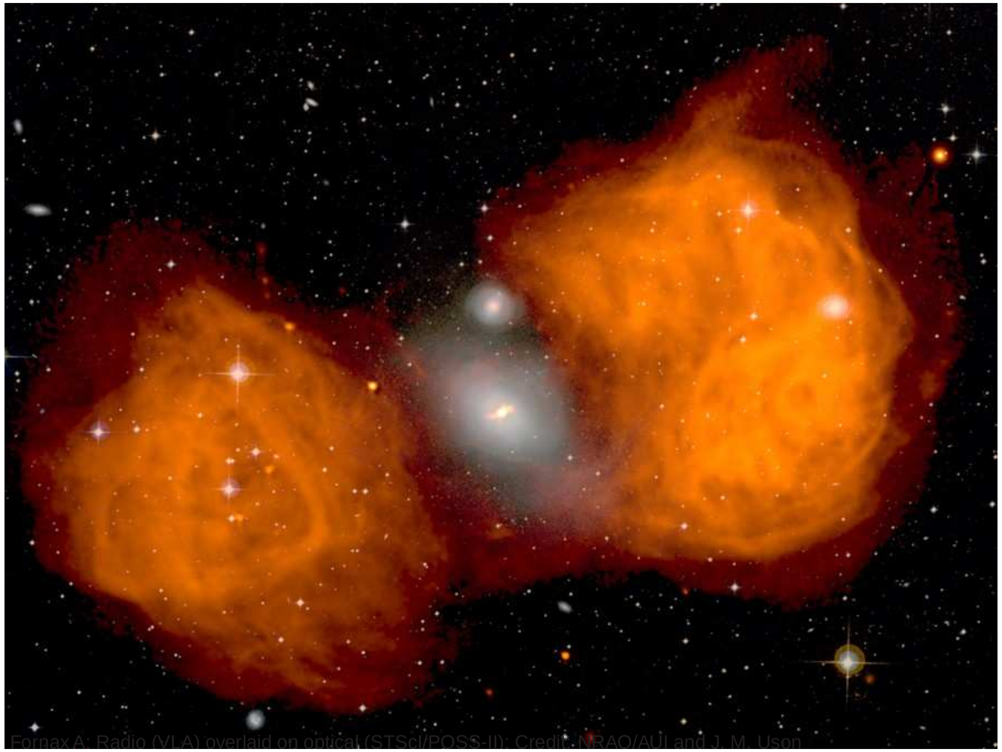

Fornax A: Radio (VLA) overlaid on optical (STScI/POSS-II); Credit: NRAO/AUI and J. M. Uson

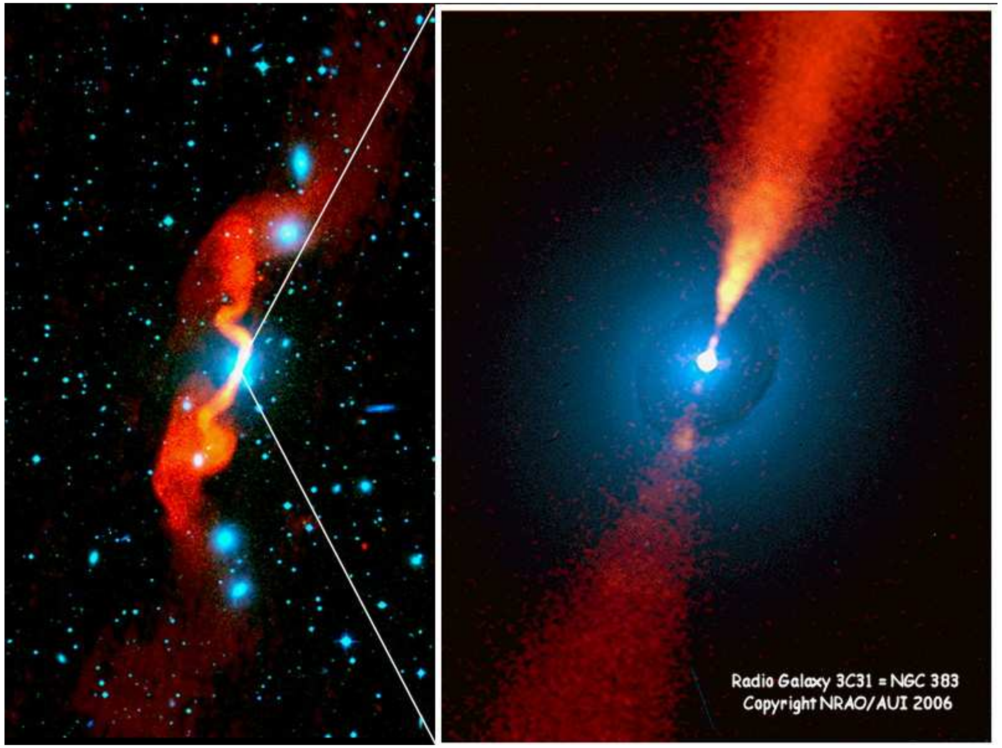

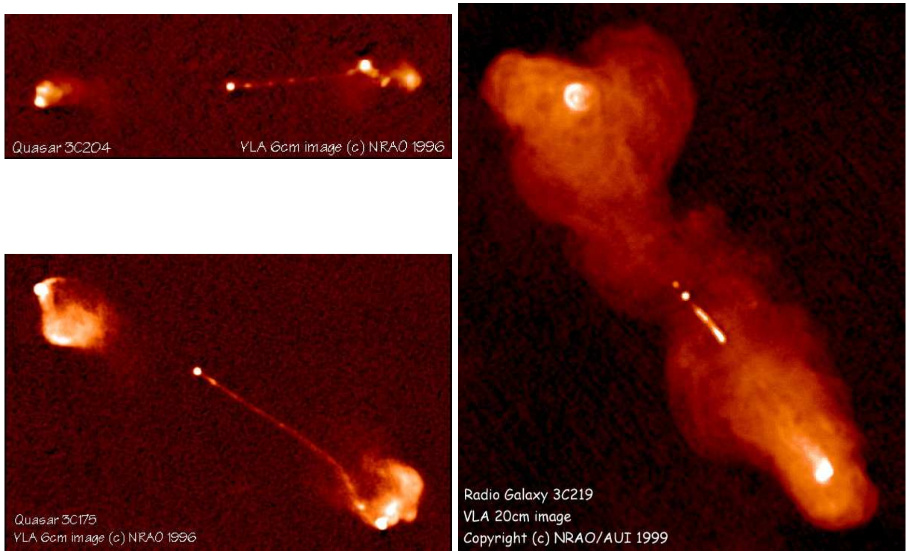

A. Bridle, `www.cv.nrao.edu/~abridle/images.htm`

Fanaroff-Riley Type 2: powerful lobe dominated doubles; jets often one-sided

Flat-Spectrum Radio Sources: Blazars

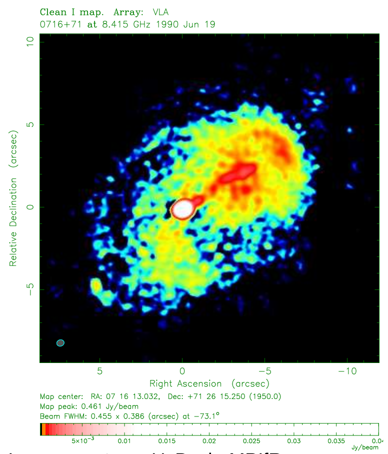

Image courtesy: U. Bach, MPIfR
0716+714: BL Lac at $z = 0.3$ (Nilsson et al., 2008)
Highly variable, core dominated object
"Fried-egg morphology": end-on view of a radio lobe?

Almost all flux density is concentrated within a few milliarcseconds-size compact jet!

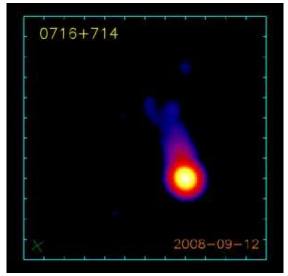

Image Courtesy: MOJAVE

"[There are] roughly equal numbers of steep-spectrum extended double-lobed sources and flat-spectrum objects that are unresolved on arc-sec scales." (Zensus, 1997)

Radio Interferometry: Longer baselines and higher frequencies yield higher resolution

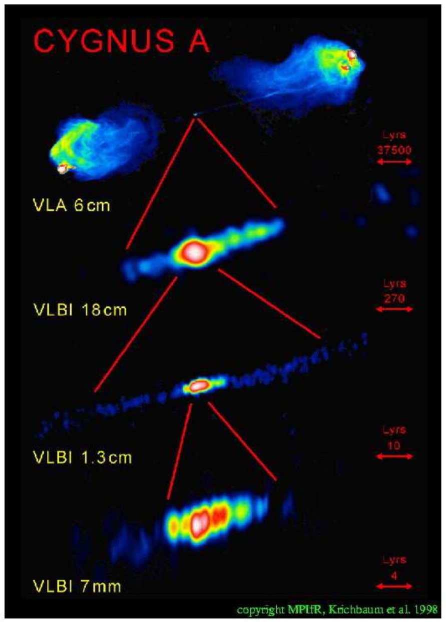

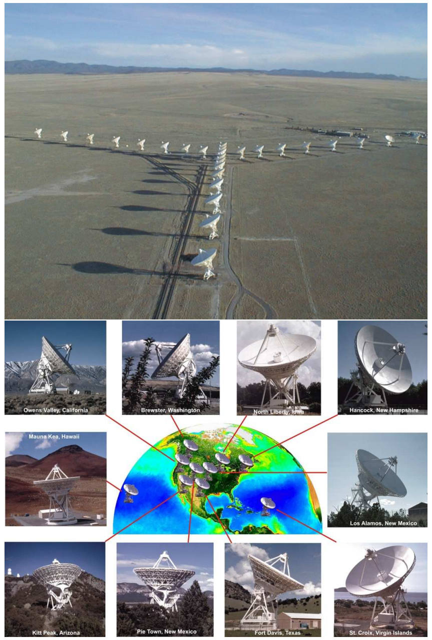

Image courtesy of MPIfR, NRAO/AUI and Earth image courtesy of the SeaWiFS Project NASA/GSFC and ORBIMAGE

Example: Cygnus A

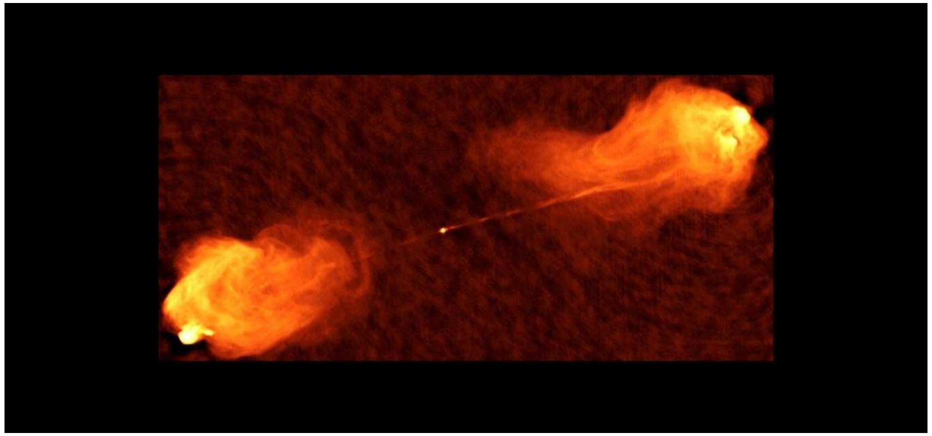

Morphology of radio galaxies: matter is transported along two channels (jets) from the center of the system (core) to the outer regions (here: lobes): What is the speed?

Apparent Superluminal Motion, I

VLBI resolution 1 mas

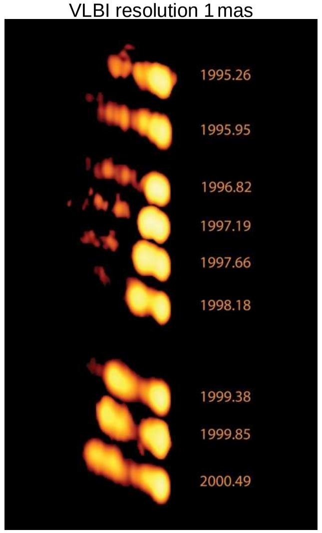

Kadler et al. (2008)

3C 111: Apparent speed of jet: $\sim 5c$

Superluminal motion: Apparent velocities of jet features ("blobs") in many AGN jets are $v > c$.

First discovered in 1971 in 3C279
(Cohen et al., 1971; Whitney et al., 1971).

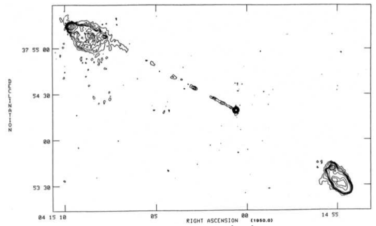

VLA resolution $\sim$ 1 arcsec

Superluminal Motion Demo:

www.physics.purdue.edu/MOJAVE/superluminal.swf

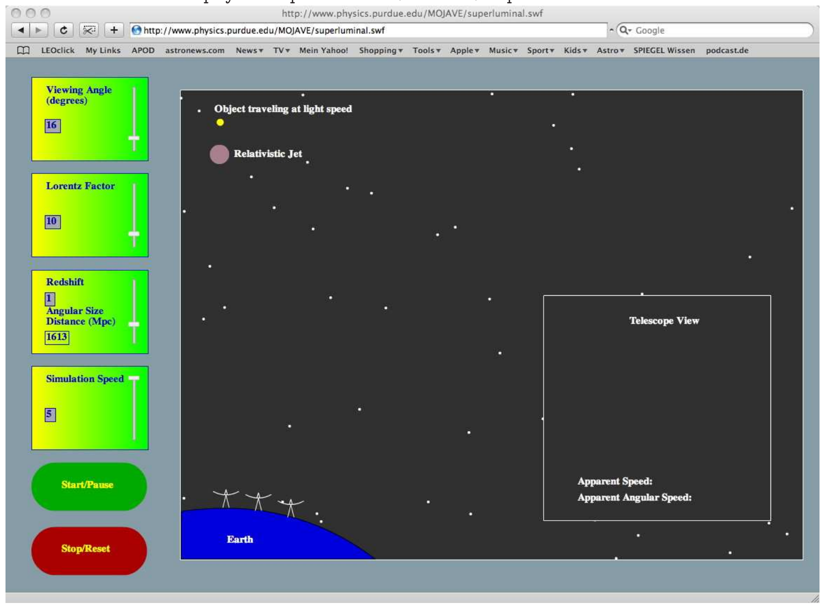

$t_1 = 0$: Blob is ejected from core and emits first photon.

Apparent Superluminal Motion, II

Movies: Examples of superluminal motion in AGN jets

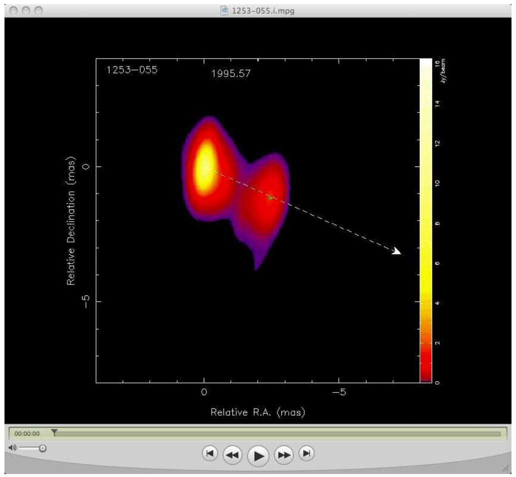

http://www.physics.purdue.edu/astro/MOJAVE/movies.html

Superluminal Motion Demo:

www.physics.purdue.edu/MOJAVE/superluminal.swf

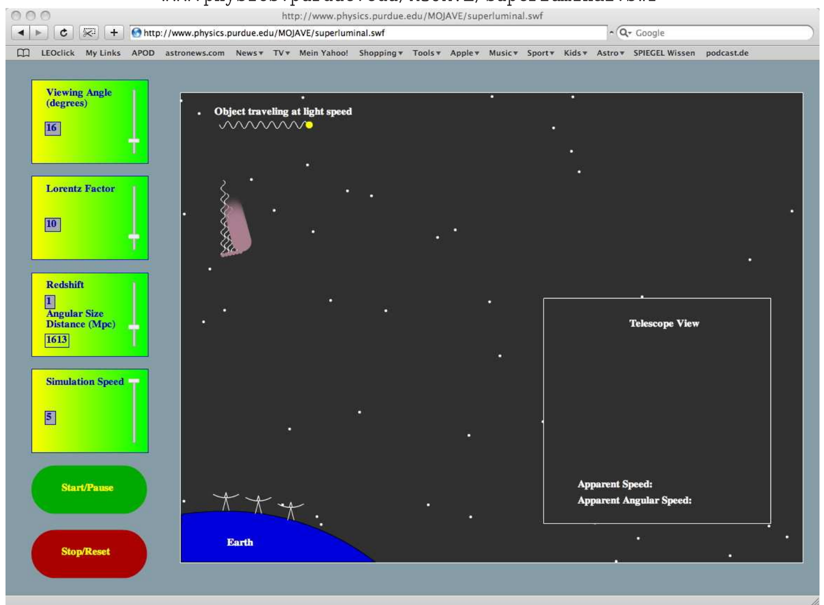

t_2: First photons and blob travel towards earth.

Superluminal Motion Demo:

www.physics.purdue.edu/MOJAVE/superluminal.swf

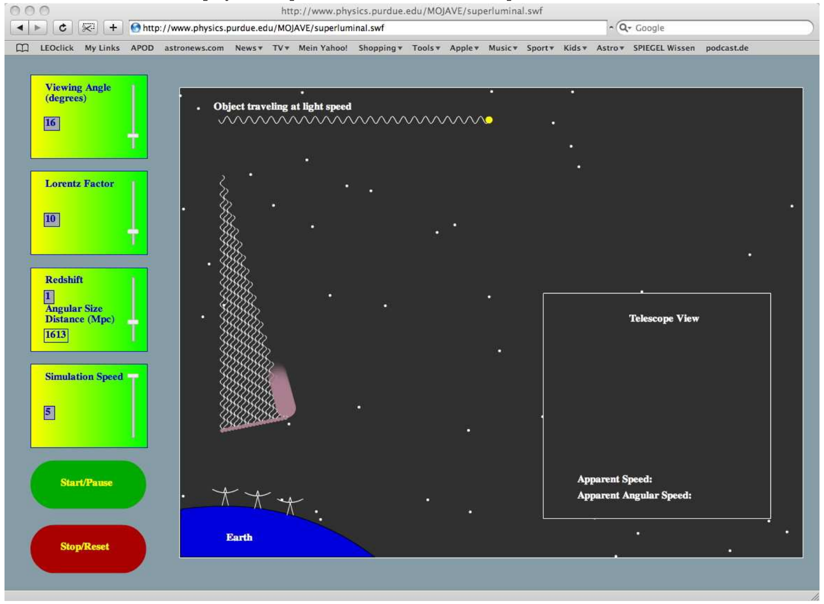

t_3: Blob almost keeps the pace of the photons.

Superluminal Motion Demo:

www.physics.purdue.edu/MOJAVE/superluminal.swf

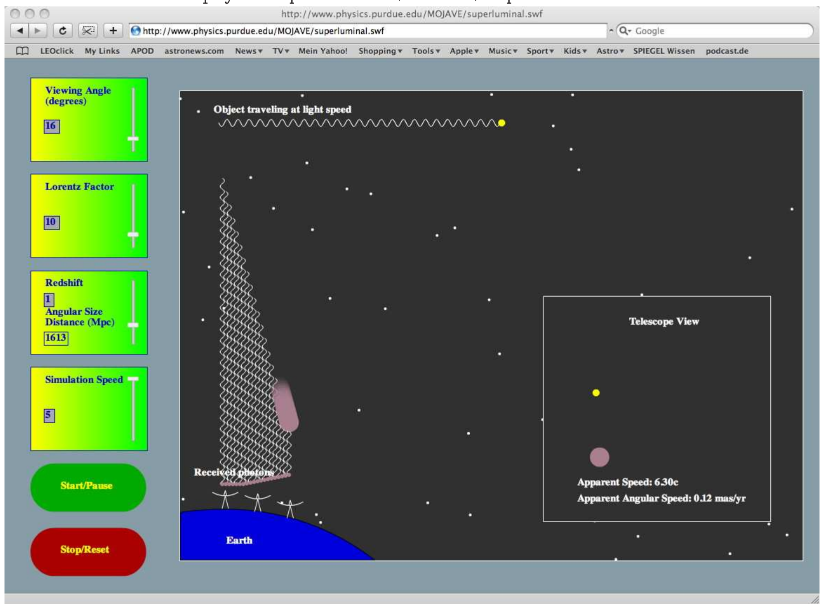

t_4: First photons arrive at telescope. Observer starts to take the time.

Superluminal Motion Demo:

www.physics.purdue.edu/MOJAVE/superluminal.swf

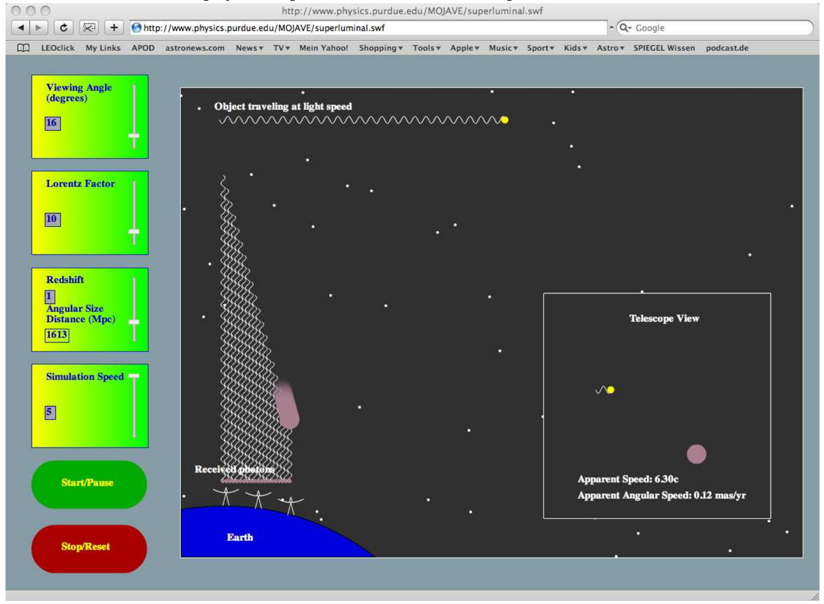

t_5: The last photons have a much shorter way to travel and arrive quickly.

Observer measures superluminal motion on the sky!

Apparent Superluminal Motion, VIII

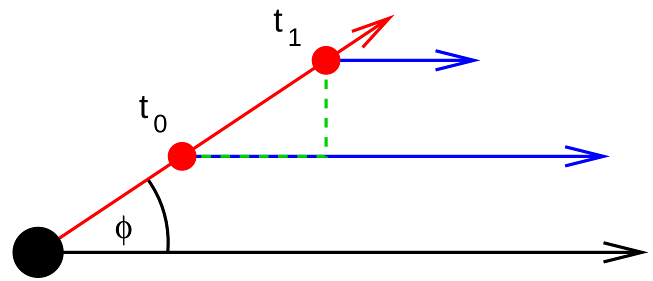

Consider blob moving towards us with speed v and angle ϕ with respect to line of sight, which emits signals at t_0 and $t_1 = t_0 + \Delta t_e$

Light travel time: Observer sees signals separated by

$$\Delta t_o = \Delta t_e - \Delta t_e \frac{v}{c} \cos\phi = \left(1 - \frac{v}{c}\cos\phi\right) \Delta t_e \tag{5.5}$$

Observed distance traveled in plane of sky:

$$\Delta \ell_\perp = v \Delta t_e \sin\phi \tag{5.6}$$

Apparent Superluminal Motion, IX

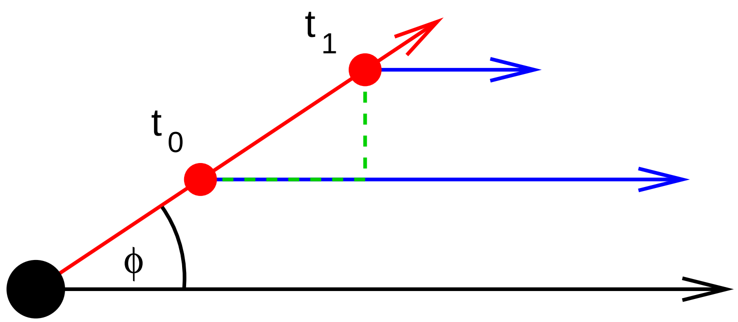

Apparent velocity deduced from observations:

$$v_{\text{app}} = \frac{\Delta\ell_\perp}{\Delta t_{\text{o}}} = \frac{v\Delta t_{\text{e}}\sin\phi}{\left(1-\frac{v}{c}\cos\phi\right)\Delta t_{\text{e}}} = \frac{v\sin\phi}{\left(1-\frac{v}{c}\cos\phi\right)} \quad (5.7)$$

$\Longrightarrow$ For v/c large and ϕ small: $v_{\text{app}} > c$

Apparent Superluminal Motion, X

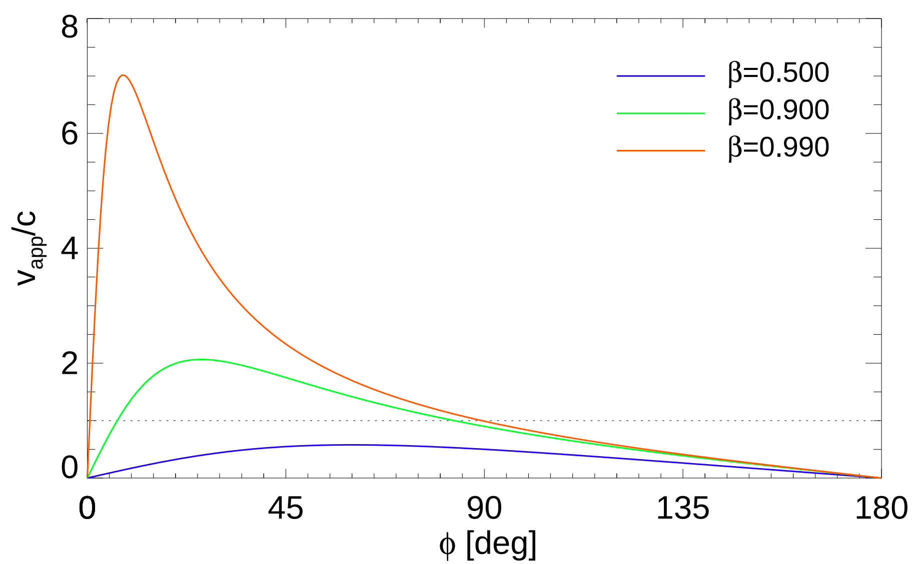

Relativistic Boosting, I

If jet plasma is moving at relativistic speeds, we have to consider also other relativistic effects.

Remember that (Doppler!)

$$\nu = \frac{1}{\Delta t_{\text{A}}} = \frac{\nu'}{\gamma\left(1-\frac{v}{c}\cos\theta\right)} \quad \text{where} \quad \gamma = \frac{1}{\sqrt{1-\frac{v^2}{c^2}}} \quad (5.8)$$

This defines the relativistic Doppler factor

$$\mathcal{D} = \frac{1}{\gamma\left(1-\frac{v}{c}\cos\theta\right)} = \frac{\sqrt{1-\beta^2}}{1-\beta\cos\theta} \quad (5.9)$$

(difference to classical Doppler factor is only the γ factor).

The Doppler factor is a strong function of the aspect angle and can become very large for $v \to c$.

Relativistic Boosting, II

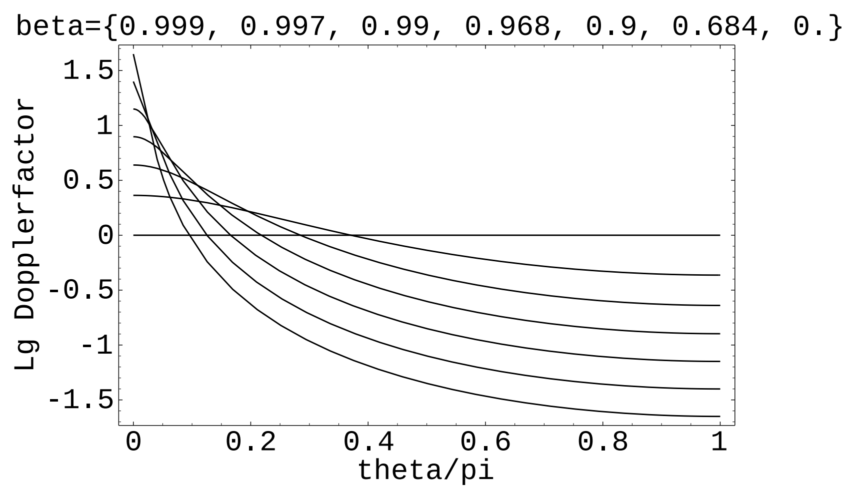

For $\theta \sim 1°$–$2°$, the Doppler factor can approach values of 100 or higher.

Relativistic Boosting, III

One can show (i.e., Rybicki & Lightman, chap. 4.9) that S_ν/ν^3 is invariant under Lorentz transformation, where S_ν is the flux density.

Therefore, observed intensity of a moving blob:

$$\frac{I(\nu_{\text{obs}})}{\nu_{\text{obs}}^3} = \frac{I(\nu_{\text{em}})}{\nu_{\text{em}}^3} \quad (5.10)$$

and

$$I(\nu_{\text{obs}}) = \nu_{\text{obs}}^3 \frac{I(\nu_{\text{em}})}{\nu_{\text{em}}^3} = \mathcal{D}^3 I(\nu_{\text{em}}) \quad (5.11)$$

Specifically, for a blob with a power law spectrum ($I(\nu) = A\nu^\alpha$):

$$I(\nu_{\text{obs}}) = \mathcal{D}^3 A \nu_{\text{em}}^\alpha = \mathcal{D}^3 A \mathcal{D}^{-\alpha} \nu_{\text{obs}}^\alpha \quad (5.12)$$

$$I(\nu_{\text{obs}}) = \mathcal{D}^{3-\alpha} I(\nu_{\text{em}}) \quad . \quad (5.13)$$

Even for relatively modest relativistic velocities, e.g., $0.97c$ ($\gamma \simeq 4$), forward flux can be boosted by a factor 1000, while it is reduced by a factor 1000 in the backward direction!

Jet One-Sidedness, I

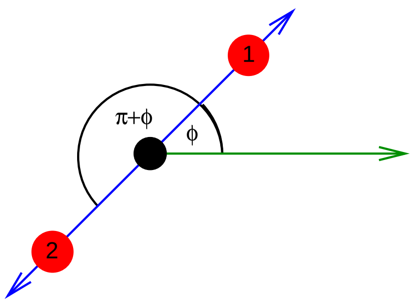

Take a source emitting blobs symmetrically in two directions.

From Eq. (5.12) the ratio of fluxes from the blobs is

$$\frac{F_1}{F_2} = \left(\frac{1+\beta\cos\phi}{1-\beta\cos\phi}\right)^{3-\alpha} \quad (5.14)$$

Even for mildly relativistic speeds and large angles, features on the approaching side are always significantly brighter than on the receding side.

Jet can be expressed as a series of blobs. But the number of blobs observed scales as the Doppler factor, such that for jets:

$$\frac{F_1}{F_2} = \left(\frac{1+\beta\cos\phi}{1-\beta\cos\phi}\right)^{2-\alpha} \quad (5.15)$$

One sidedness of jets is a relativistic effect!

Jet One-Sidedness, II

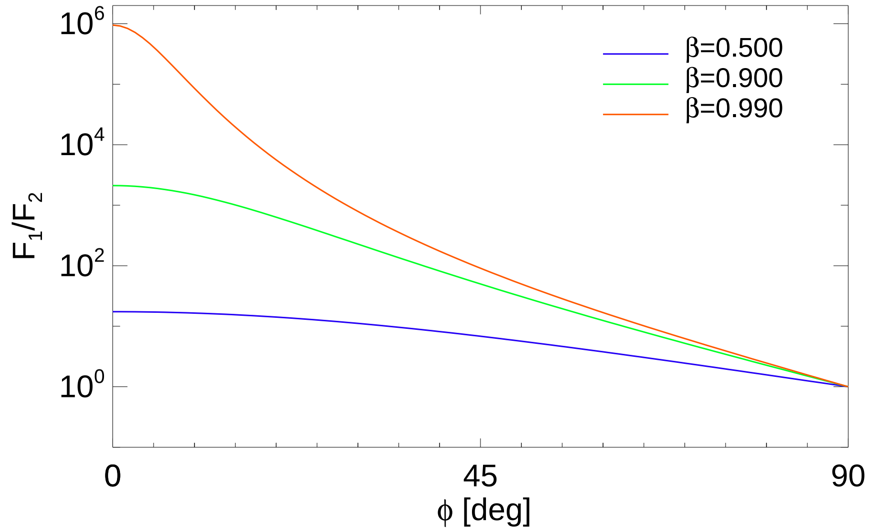

Survey and monitoring of extragalactic jets on parsec scales with the VLBA since 1995

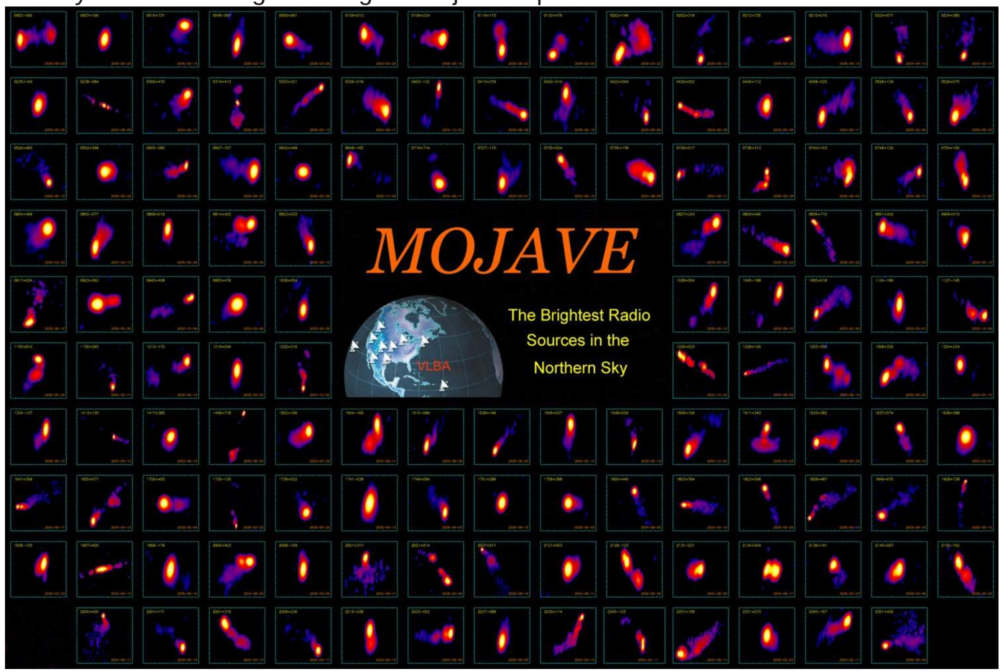

http://www.physics.purdue.edu/astro/MOJAVE/

Kinematics of Relativistic Jets, II

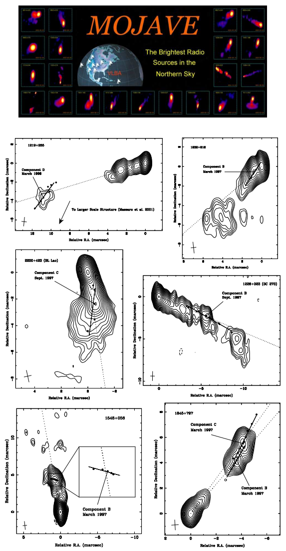

- **MOJAVE**: **M**onitoring **O**f **J**ets in **A**ctive galactic nuclei with **V**LBA **E**xperiments; (Lister et al., 2009, and therein)
- Wavelength $\lambda = 2$ cm (15 GHz)
- Statistically complete sub-sample: All flat-spectrum ($\alpha < 0.5$) sources whose compact flux density ever reached 1.5 Jy (2 Jy for southern sources)
- Extended sample includes all known gamma-ray blazars (newly detected *Fermi* sources to be added as of January 2009)
- Results, images and movies at `http://www.physics.purdue.edu/astro/MOJAVE/`
- Observing strategy optimized for each individual source (fast sources are observed every month, slower sources less frequently)

Kinematics of Relativistic Jets, III

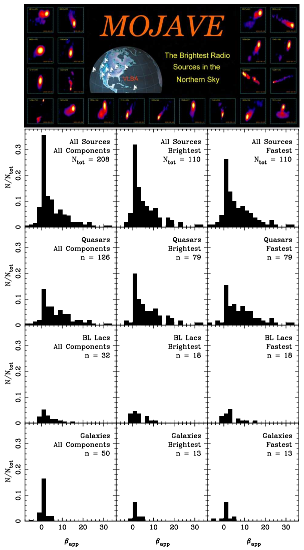

MOJAVE Results:

- Distribution of observed velocities typically between 0 and 15c: Quasars: tail up to $\beta_{\text{app}} \sim 34$; BL Lacs and galaxies: mainly $\beta \lesssim 6$
- In the same jet, different components tend to have similar speeds; but there are exceptions
- In many sources, bent trajectories are seen, which do not back-extrapolate to the core: no cannon-balls!
- Observed pattern speed does not necessarily agree with beam speed
- Most of the flux-density originates in still unresolved regions smaller than 0.05 mas
- High-energy (gamma-ray) emitters have faster and more compact jets

(Kellermann et al., 2004; Kovalev et al., 2005; Cohen et al., 2007)

High Energy Radiation from Jets, I

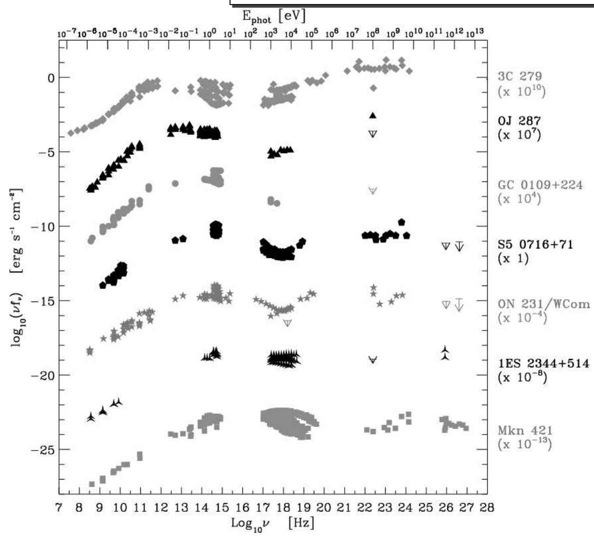

Sneak-preview of “blazar sequence” (Fiorucci et al., 2004)

Radio-loud AGN emit across the whole electromagnetic spectrum!

This holds for the compact and large-scale jets of both quasars and radio galaxies.

How can we transfer the power of the compact jet into high-energy emission?

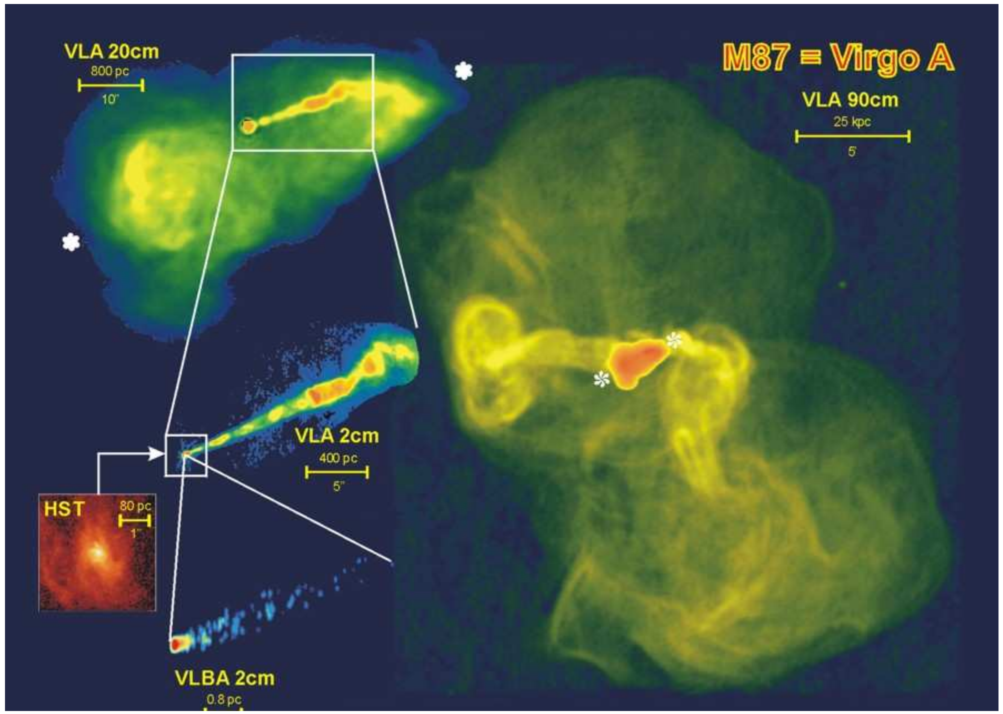

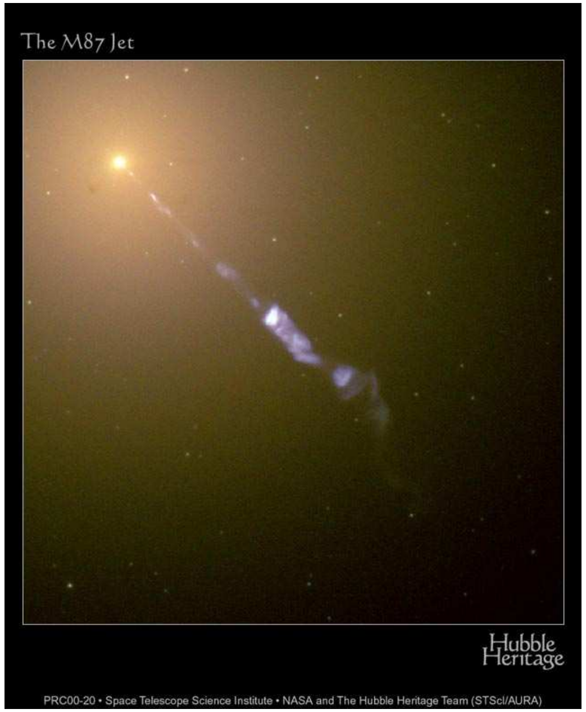

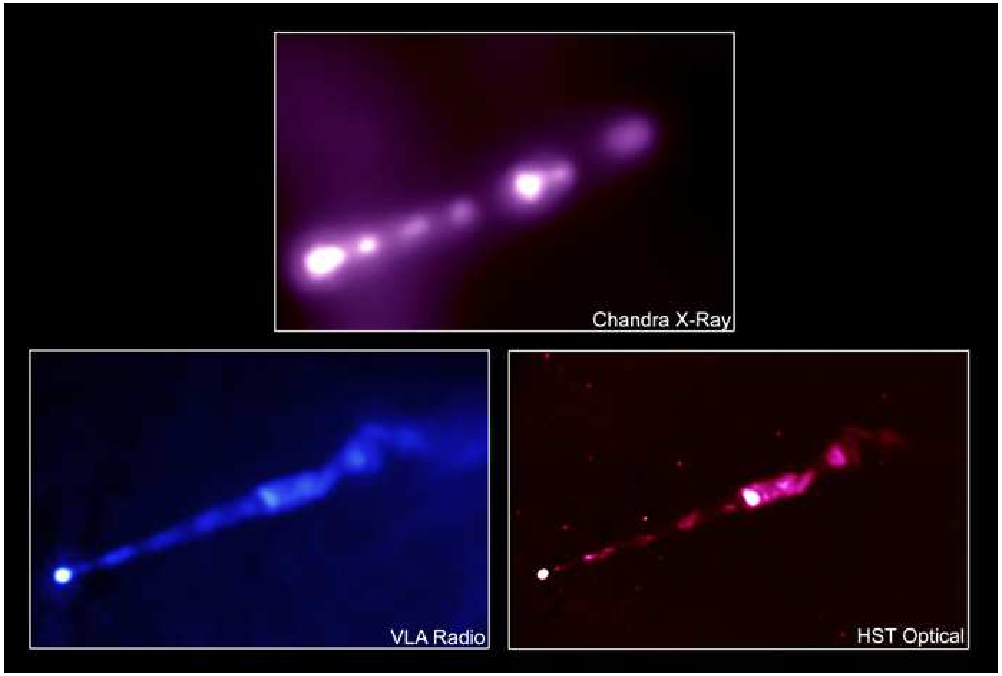

High Energy Radiation from Jets, VI

Blazars are broadband emitters and the most natural targets for multi-wavelength astronomy!

The expression *Blazar* was first used in 1978 to express that optically violently variable quasars (OVVs) and BL Lac objects share their extreme variability characteristics.

Although first detected in optical and radio, a large fraction of their total energy output is at high energies: hard X-rays, γ-rays, and up to the very high energy (VHE) regime.

The *Compton Gamma-Ray Observatory (CGRO)* with its main detector EGRET revolutionized blazar research by the finding that blazars are the dominant population of extragalactic gamma-ray sources.

The short variability time scales (days!) indicate that the gamma-ray emission comes from beamed plasma (jets) to avoid photon-photon pair production in otherwise too dense gamma photon fields.

Prototypical Example: 3C 273, I

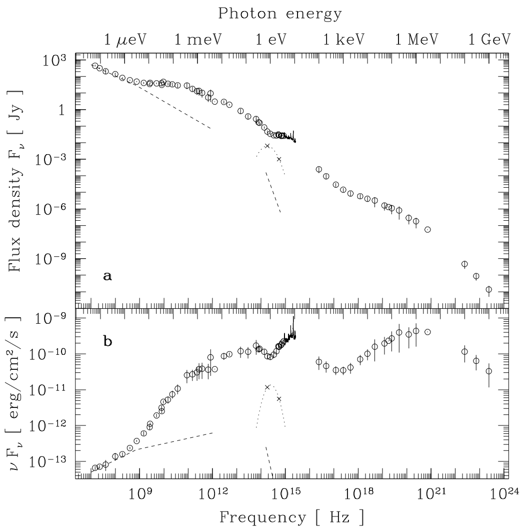

(Türler et al., 1999)

3C 273:

- First detected and brightest (and probably best studied) quasar
- Bright throughout the whole electromagnetic spectrum
- Prominent "big blue bump"
- Huge public database: Türler et al. (1999), Soldi et al. (2008)

Prototypical Example: 3C 273, II

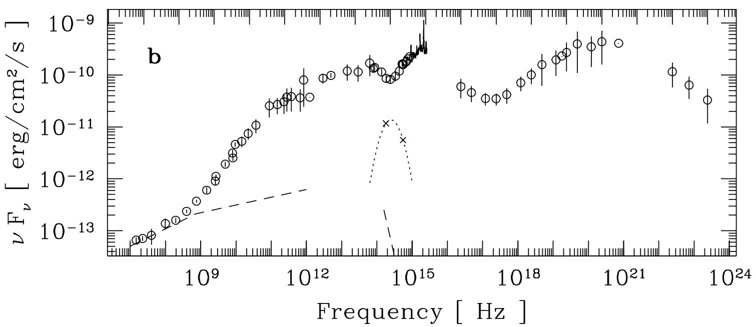

- Radio: low-frequency emission from large-scale jet; high-frequencies from compact jet (flat spectrum in F_ν)
- up to IR: synchrotron emission from compact jet (possibly plus dust component (dusty torus?))
- "big blue bump" in the optical: accretion disk (?)
- X-rays and up: inverse Compton emission (possibly from multiple seed photon fields)

Broadband Emission Models, I

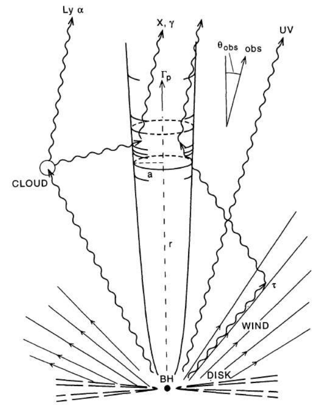

Geometry in leptonic models (Sikora et al., 1994)

General agreement that the low-energy component is jet-synchrotron emission.

Models for production of high energy photons:

- Leptonic models: inverse Compton scattering of soft seed photons by the relativistic electrons responsible for the synchrotron emission. Seed photons are
  - the synchrotron photons themselves (SSC, e.g. Tavecchio et al., 1998), or
  - external, e.g., from the accretion disk or the BLR (EC, e.g. Sikora et al., 1994)
- Hadronic models: reactions involving high-energy protons (hadron-hadron or photon-hadron collisions, pair production and subsequent e^+e^- cascades (e.g. Mannheim, 1993))

Hadronic models are attractive because they can explain the observed ultra-high energetic (UHE) cosmic rays but they have problems explaining the observed X-ray spectra.

Broadband Emission Models, II

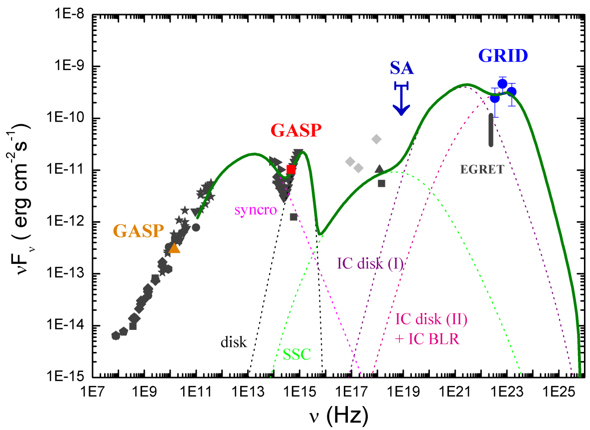

SED of PKS B 1510−089 (Pucella et al., 2008)

Modeling the broadband SED:

- Consider primary components: synchrotron, disk, scattered BLR emission
- Inverse-Compton components from SSC and EC (of the dominating external photon fields)

Prototypical Example: 3C 273 (continued), I

Almost 40 years of multiwavelength observations of 3C 273 (Soldi et al., 2008)

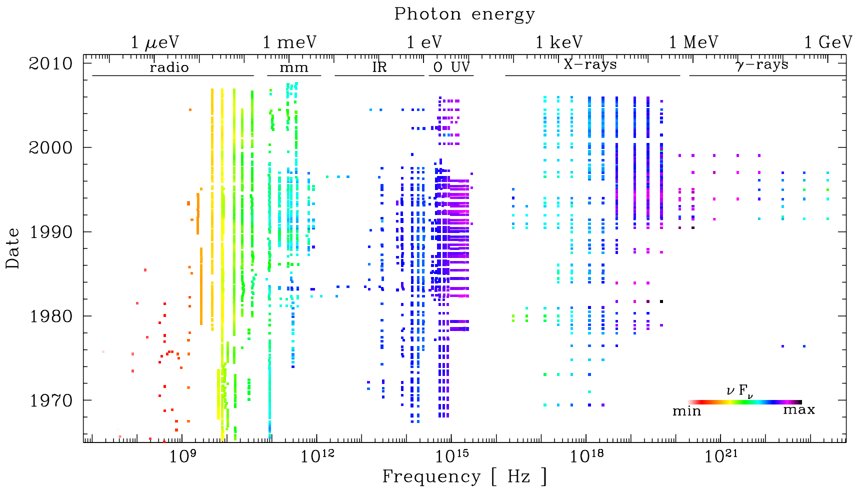

Prototypical Example: 3C 273 (continued), II

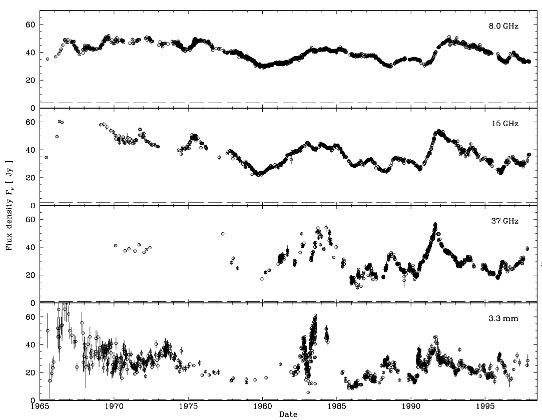

(Türler et al., 1999)

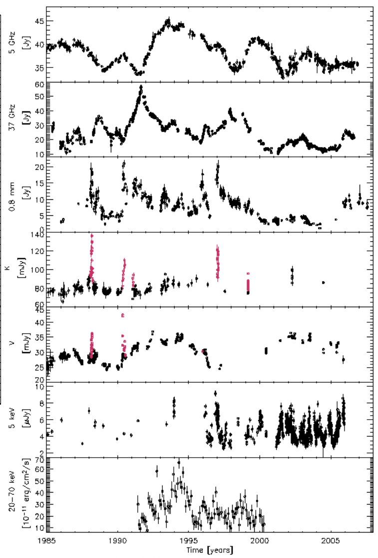

(Soldi et al., 2008)

Variability at all wavelengths but with different time scales and amplitudes ⇒ multiple emission components and/or mechanisms

Prototypical Example: 3C 273 (continued), III

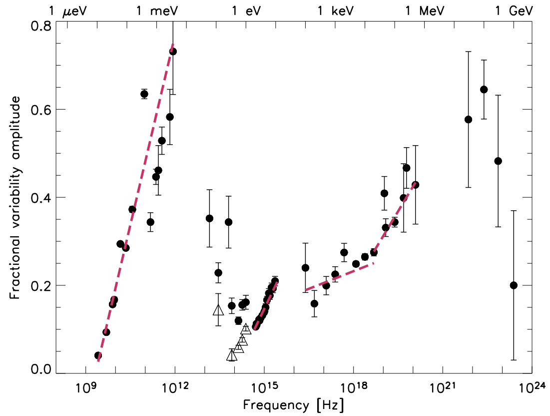

Fractional variability amplitude:

$$F_{\text{var}} = \sqrt{\frac{S^2 - \bar{\varepsilon}^2}{\bar{x}^2}} \qquad (5.16)$$

where: S^2: sample variance of the light curve, $\bar{x}$: average flux, and $\bar{\varepsilon}^2 = \frac{1}{N}\sum_i \varepsilon_i^2$: mean of the squared measurement uncertainties.

The fractional variability amplitude strongly depends on frequency, rising towards the high-energy end of the synchrotron and IC components. Less-variable IR emission (from dust?).

Prototypical Example: 3C 273 (continued), IV

Almost 40 years of multiwavelength observations of 3C 273 (Soldi et al., 2008)

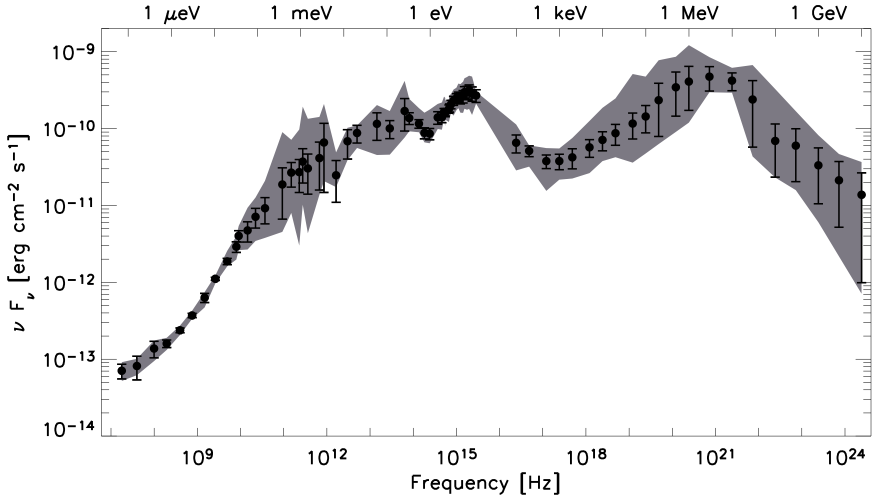

Prototypical Example: 3C 273 (continued), V

A historic jet-emission minimum (Türler et al., 2006)

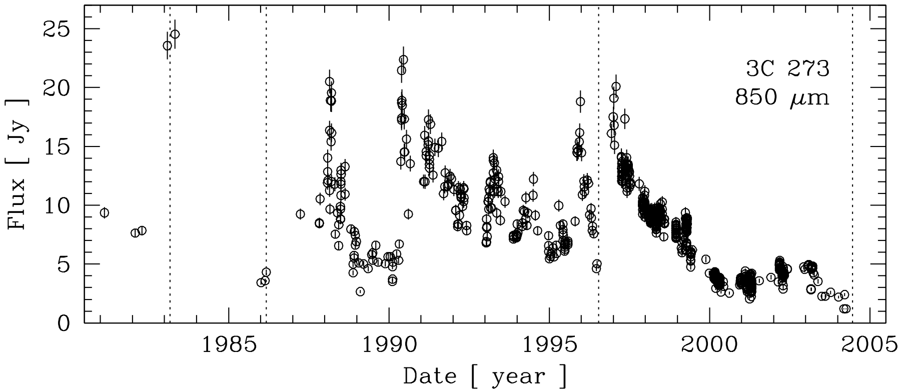

Prototypical Example: 3C 273 (continued), VI

A historic jet-emission minimum (Türler et al., 2006)

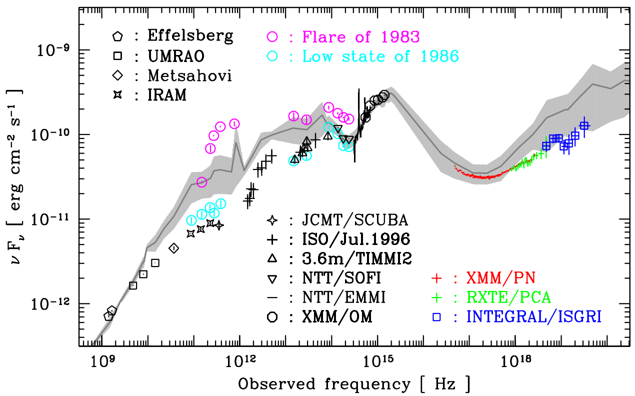

When the jet is weak, Seyfert-like features appear: Thermal dust, iron line; blue bump not directly coupled to jet emission

The Blazar Sequence, I

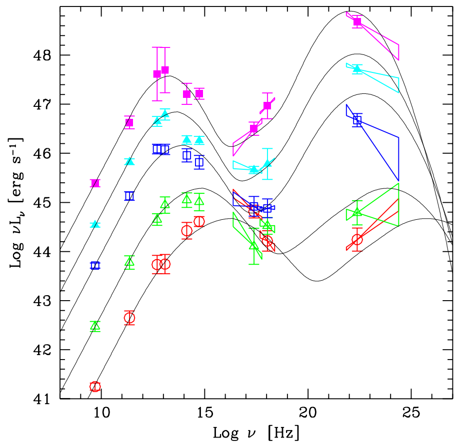

Construction of average blazar SEDs binned according to radio luminosity (Fossati et al., 1998; Donato et al., 2001).

For all luminosity classes, there are two broad peaks

- LBL objects: High-luminosity sources peak at lower frequencies (IR and MeV range)
- HBL objects: Low-luminosity sources peak at higher frequencies (UV/X-rays and up to TeV energies)

(Donato et al., 2001, based on Fossati et al. 1998)

The Blazar Sequence, II

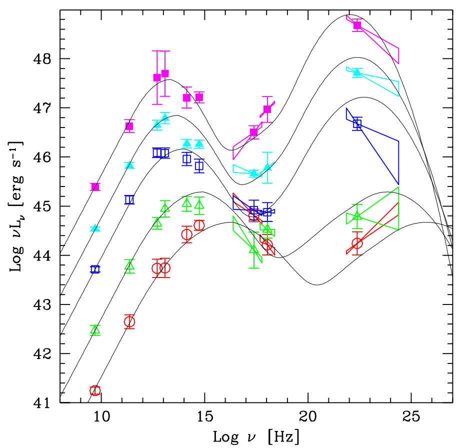

Analytic parametrization:

- Peak frequencies are inversely proportional to luminosity
- Constant ratio of the two peak frequencies
- Strength of the second peak proportional to luminosity

Attention: EGRET detected preferentially blazars during outbursts ⇒ Bias in high-energy data.

There is an ongoing debate on the validity of the blazar sequence. A (small) number of sources does not fit in.

(Donato et al., 2001, based on Fossati et al. 1998)

Blazars at γ-Ray Energies, I

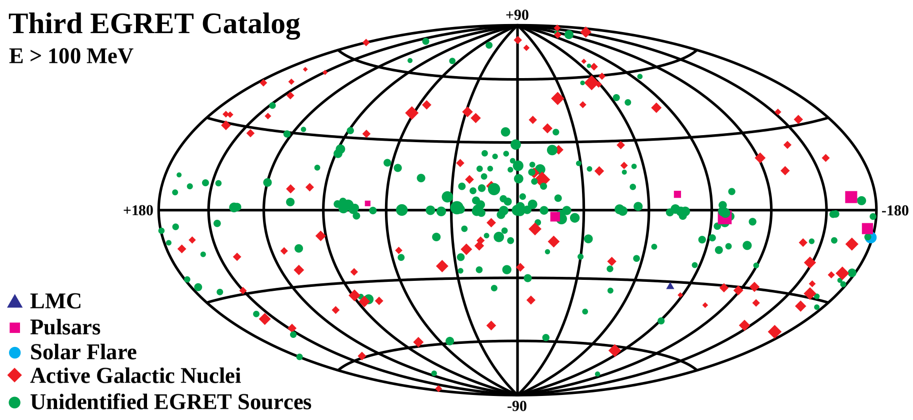

Hartman et al. (1999): 271 sources – 5 pulsars, 1 solar flare, 93 blazars (66 high confidence, 27 possible associations), 1 radio galaxy, 1 normal galaxy, and 170 (!) unidentified sources.

Blazars at γ-Ray Energies, II

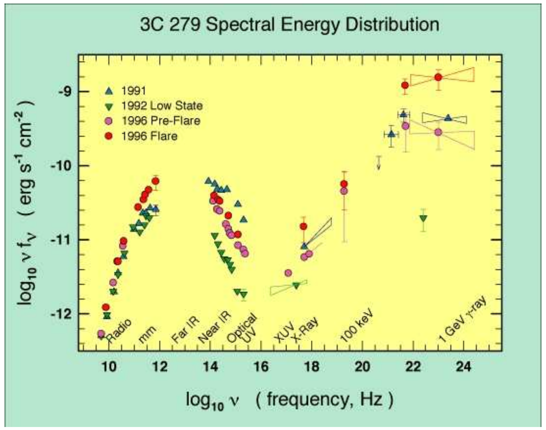

Courtesy: EGRET Team

Blazar SED dominated by γ-ray emission.

Example 3C 279:

- Surprise! (observation was looking for 3C 273)
- Became the prototypical γ-ray blazar through the whole EGRET mission

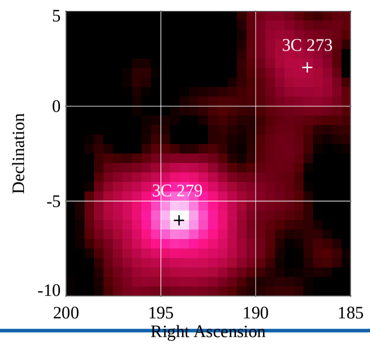

Blazars at γ-Ray Energies, III

The elusive gamma-ray regime is now much better covered than ever before:

Agile launched in April 2007. Now in routine pointed observations mode.

`http://agile.rm.iasf.cnr.it/`

GLAST (Gamma Ray Large Area Space Telescope) launched in June 2008. Now renamed to *Fermi Gamma-Ray Space Telescope* and in routine all-sky monitoring mode.

`http://fermi.gsfc.nasa.gov/`

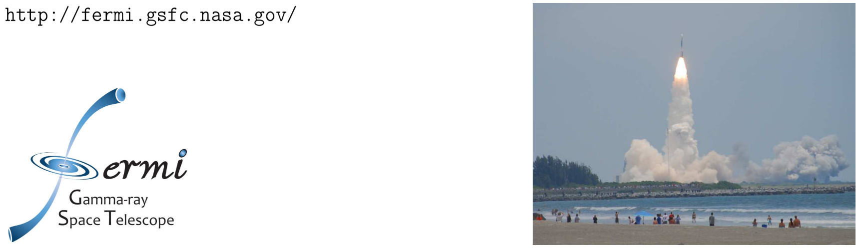

Blazars at γ-Ray Energies, IV

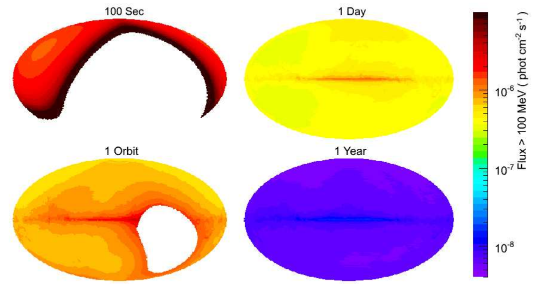

Atwood et al. (2009)

Primary observing mode of the LAT is *survey mode*:

- Full sky coverage every 2 orbits (3 hours)
- $\sim$ Uniform exposure after a couple of orbits
- Sensitivity of previous γ-ray missions reached within $\sim$1 week

Comparison with EGRET:

- Very large field of view ($\sim$ 20 % of the sky)
- Broadband (20 MeV – >300 GeV)
- PSF <1 degree (energy dependent)
- Effective area >8000 cm^2

Overall: Factor > 30 improvement in sensitivity!

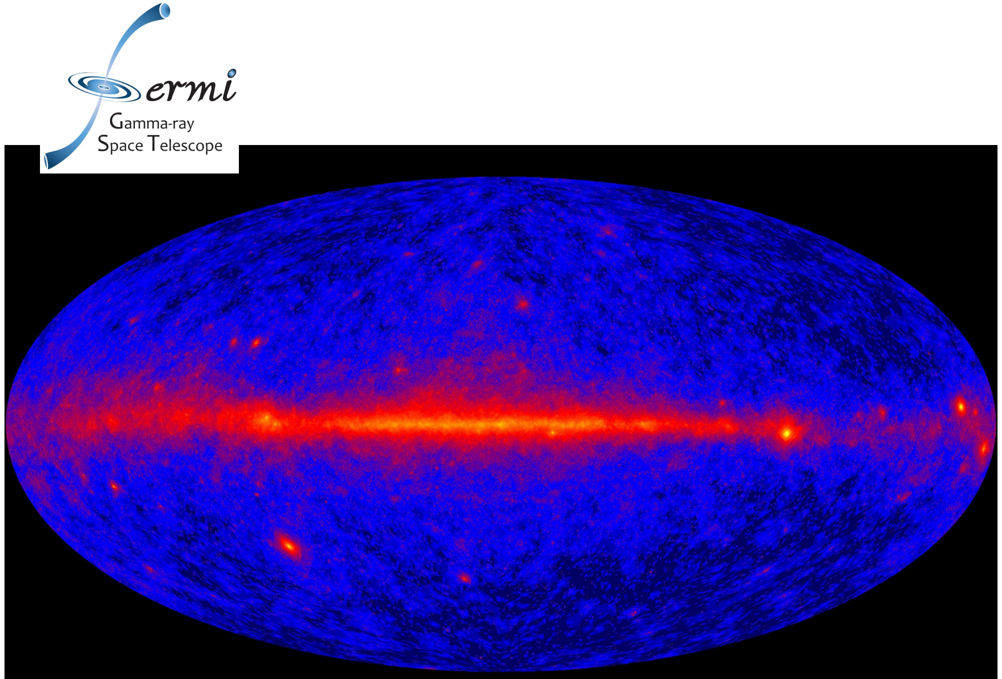

1st-Light Image of the *Fermi* Gamma-ray Space Telescope
(one week of data in August 2008)

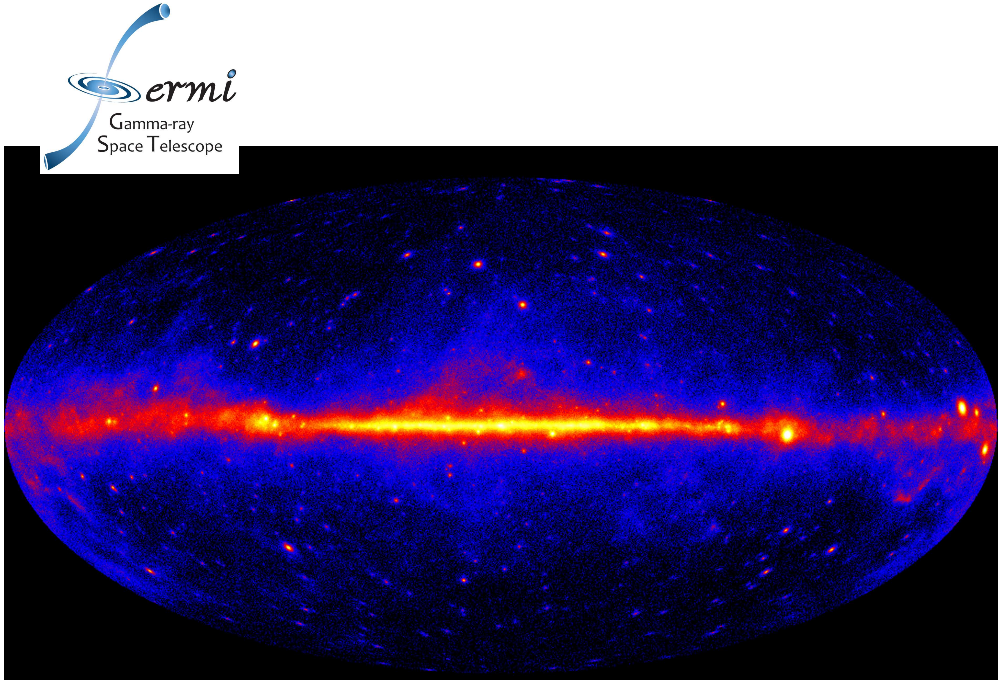

One-Year Image of the *Fermi* Gamma-ray Space Telescope
(2008/09)

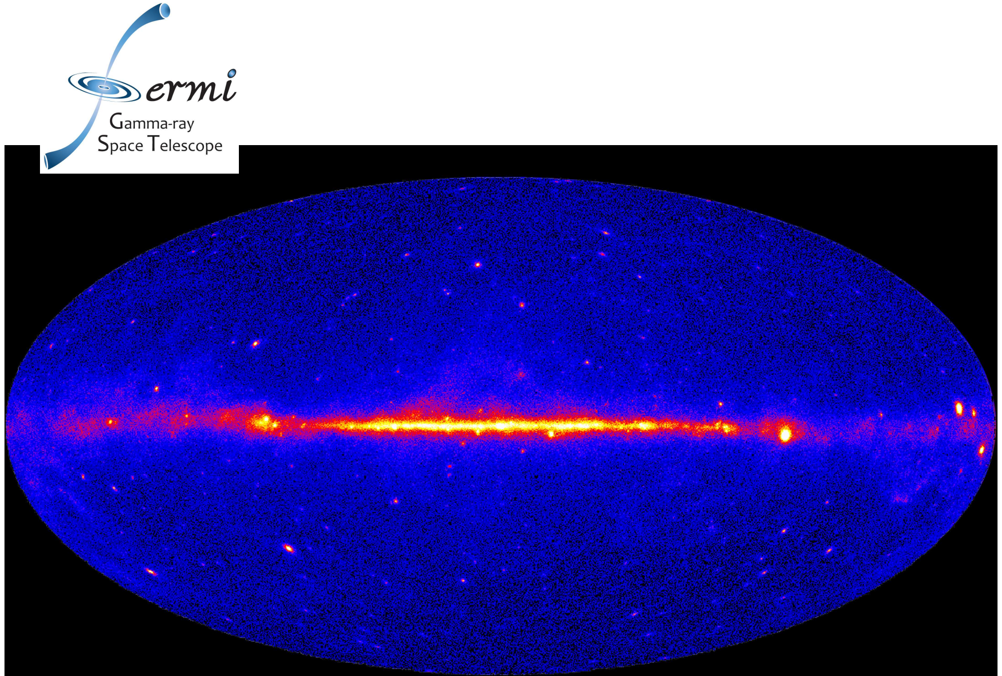

3-month Image of the *Fermi* Gamma-ray Space Telescope
(August–October 2008)

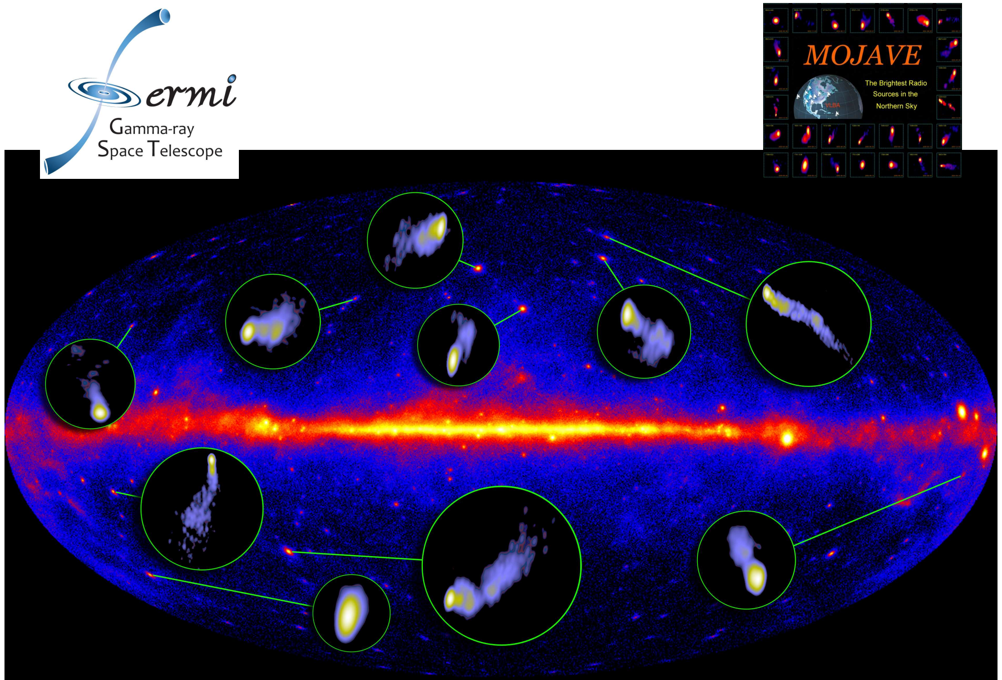

High galactic-latitude gamma-ray point sources are
flat-spectrum radio quasars and BL Lac objects

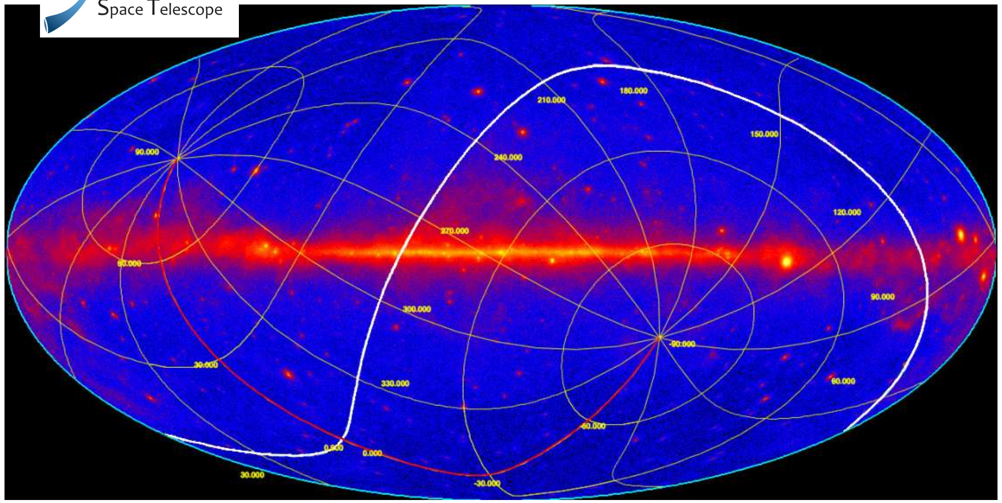

All-sky astronomy is tricky from the ground!

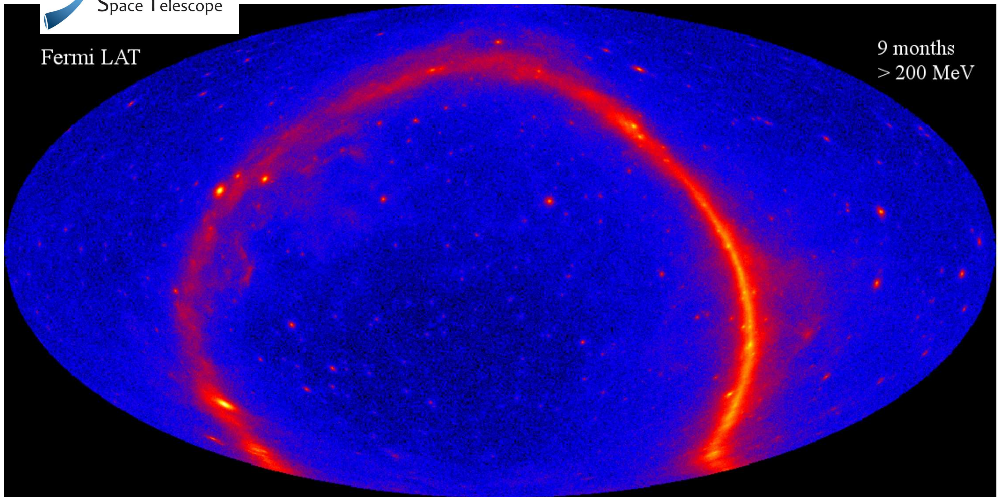

All-sky *Fermi* γ-ray image in celestial coordinates

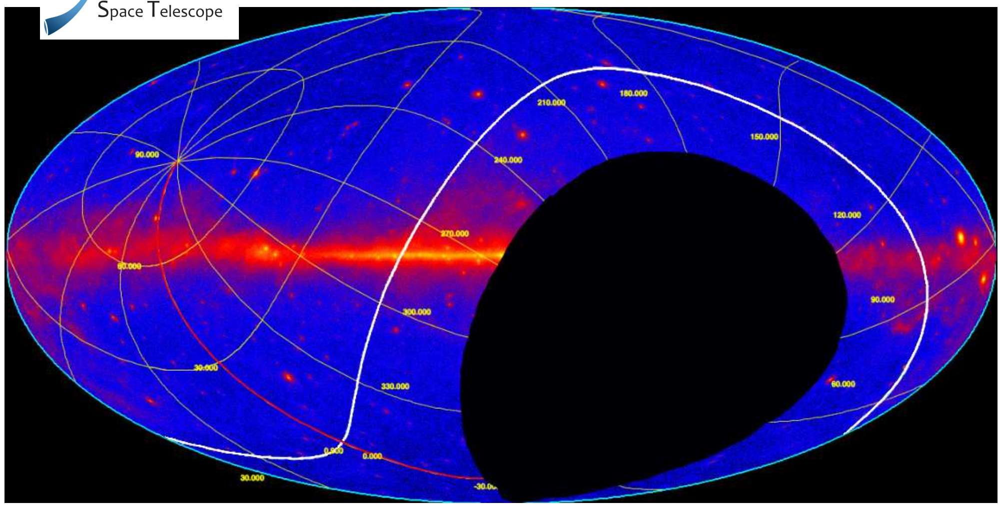

One third of the sky is not observable for
Northern-Hemisphere Telescopes!

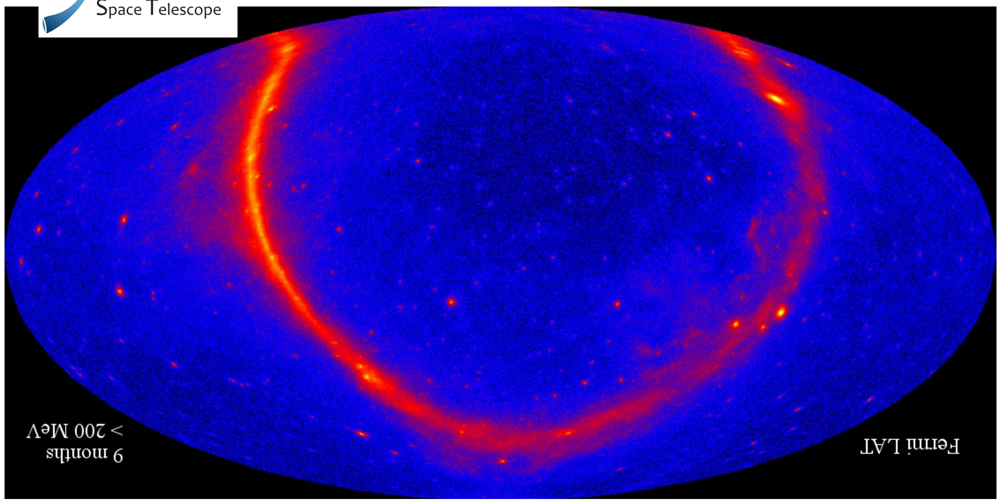

Austral View of *Fermi* γ-ray sky

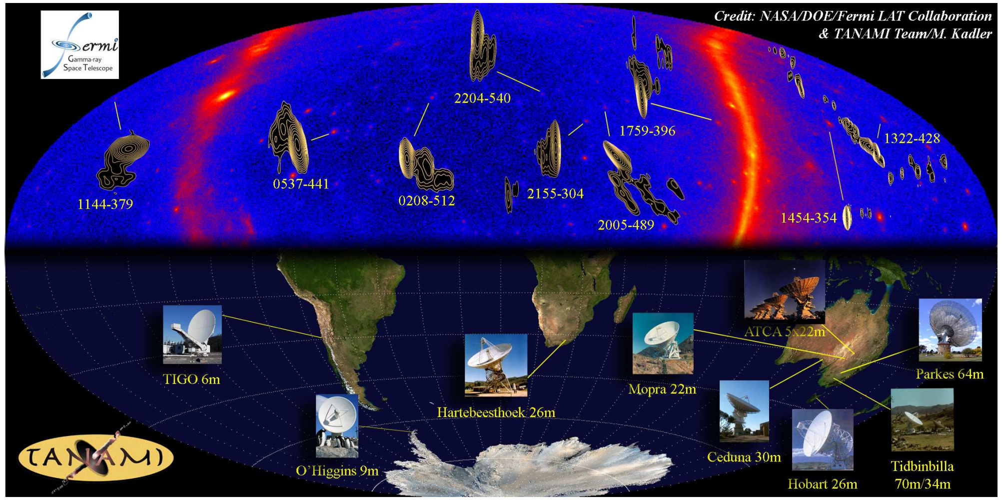

TANAMI (Tracking Active Galactic Nuclei with Austral Milliarcsecond Interferometry)
`http://pulsar.sternwarte.uni-erlangen.de/tanami`

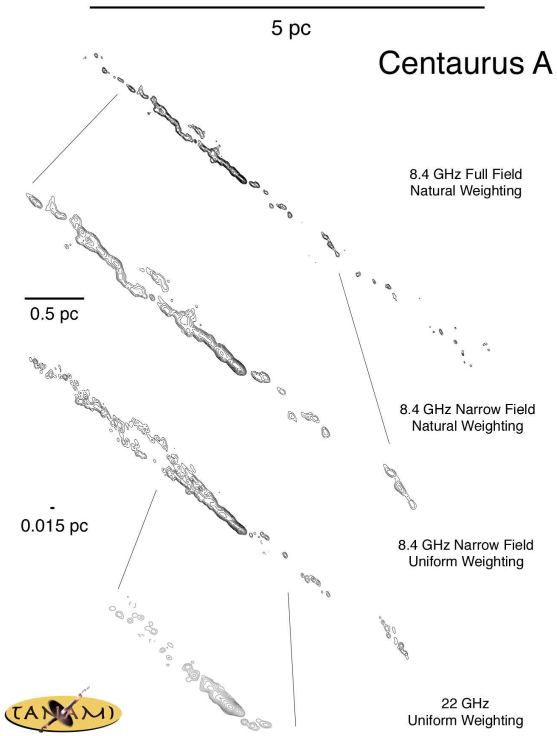

Blazars at Very High Energies

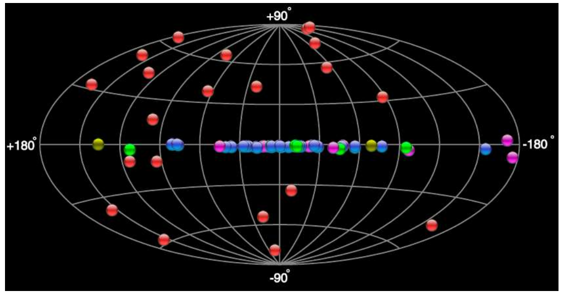

The blazar sequence predicts a dominance of HBL objects at very high energies. This is confirmed by recent blazar detections of TeV telescopes (H.E.S.S., MAGIC, VERITAS, CANGAROO):

- Currently 22 HBL objects detected and only two LBL objects (W Comae and BL Lac; check `http://tevcat.uchicago.edu/` for updated lists)
- Only non-blazar TeV source: M 87

Blazars at Very High Energies

TeV blazars are weak radio sources, because the cm-range is so far left of their synchrotron peak and because they are low-luminosity objects. Similarly, they are bright X-ray sources and relatively weak in the MeV/GeV range.

Despite their variability and SEDs require very high Doppler factors, VLBI measures slow jets (barely superluminal Piner et al., 2008, and references therein) $\Rightarrow$ 1) extremely small angles or 2) jet deceleration from the "blazar scale" to the "VLBI scale", or 3) another sign of jet-stratification (spine-sheath structure).

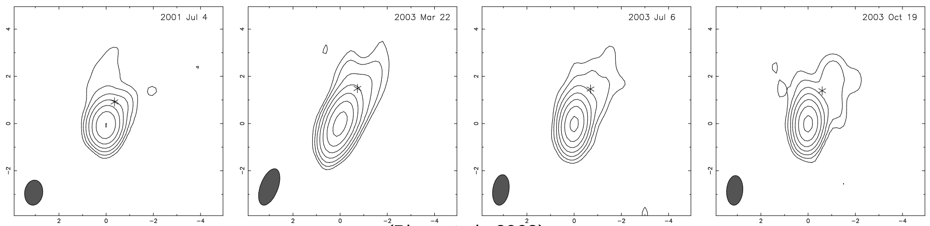

(Piner et al., 2008)

Atwood W.B., Abdo A.A., Ackermann M., et al., 2009, ApJ 697, 1071

Baade W., Minkowski R., 1954, ApJ 119, 206

Bianchi S., Matt G., Balestra I., et al., 2004, A&A 422, 65

Boller T., Tanaka Y., Fabian A., et al., 2003, MNRAS 343, L89

Cohen M.H., Cannon W., Purcell G.H., et al., 1971, ApJ 170, 207

Cohen M.H., Lister M.L., Homan D.C., et al., 2007, ApJ 658, 232

Condon J.J., Cotton W.D., Greisen E.W., et al., 1998, AJ 115, 1693

Donato D., Ghisellini G., Tagliaferri G., Fossati G., 2001, A&A 375, 739

Fabian A.C., Miniutti G., Gallo L., et al., 2004, MNRAS 353, 1071

Fabian A.C., Vaughan S., Nandra K., et al., 2002, MNRAS 335, L1

Fiorucci M., Ciprini S., Tosti G., 2004, A&A 419, 25

Fossati G., Maraschi L., Celotti A., et al., 1998, MNRAS 299, 433

García-Lorenzo B., Mediavilla E., Arribas S., 1999, ApJ 518, 190

Guainazzi M., Matt G., Molendi S., et al., 1999, A&A 341, L27

Hartman R.C., Bertsch D.L., Bloom S.D., et al., 1999, ApJS 123, 79

Iwasawa K., Fabian A.C., Reynolds C.S., et al., 1996, MNRAS 282, 1038

Iwasawa K., Miniutti G., Fabian A.C., 2004, MNRAS 355, 1073

Jiménez-Bailón E., Piconcelli E., Guainazzi M., et al., 2005, A&A 435, 449

Kadler M., Ros E., Perucho M., et al., 2008, ApJ 680, 867

Kellermann K.I., Lister M.L., Homan D.C., et al., 2004, ApJ 609, 539

Kovalev Y.Y., Kellermann K.I., Lister M.L., et al., 2005, Astron. J. 130, 2473

5–108

Kuehr H., Witzel A., Pauliny-Toth I.I.K., Nauber U., 1981, A&A 45, 367

Laing R.A., Bridle A.H., 1987, MNRAS 228, 557

Lee J.C., Fabian A.C., Brandt W.N., et al., 1999, MNRAS 310, 973

Lister M.L., Aller H.D., Aller M.F., et al., 2009, Astron. J. 137, 3718

Longinotti A.L., Cappi M., Nandra K., et al., 2003, A&A 410, 471

Mannheim K., 1993, A&A 269, 67

Matt G., Porquet D., Bianchi S., et al., 2005, A&A 435, 867

McHardy I.M., Gunn K.F., Uttley P., Goad M.R., 2005, MNRAS 359, 1469

McHardy I.M., Koerding E., Knigge C., et al., 2006, Nat 444, 730

McHardy I.M., Papadakis I.E., Uttley P., et al., 2004, MNRAS 348, 783

Nilsson K., Pursimo T., Sillanpää A., et al., 2008, A&A 487, L29

Piner B.G., Pant N., Edwards P.G., 2008, ApJ 678, 64

Porquet D., Reeves J.N., 2003, A&A 408, 119

Pucella G., Vittorini V., D'Ammando F., et al., 2008, A&A 491, L21

Reeves J.N., Turner M.J.L., Pounds K.A., et al., 2001, A&A 365, L134

Seyfert C.K., 1943, ApJ 97, 28

Shu F.H., 1991, The Physics of Astrophysics, Vol. I. Radiation, University Science Books, Mill Valley, CA

Sikora M., Begelman M.C., Rees M.J., 1994, ApJ 421, 153

Soldi S., Türler M., Paltani S., et al., 2008, A&A 486, 411

Tanaka Y., Nandra K., Fabian A.C., et al., 1995, Nat 375, 659

Tavecchio F., Maraschi L., Ghisellini G., 1998, ApJ 509, 608

5–108

Türler M., Chernyakova M., Courvoisier T.J.L., et al., 2006, A&A 451, L1

Türler M., Paltani S., Courvoisier T.J.L., et al., 1999, A&AS 134, 89

Urry C.M., Padovani P., 1995, PASP 107, 803

Whitney A.R., Shapiro I.I., Rogers A.E.E., et al., 1971, Science 173, 225

Wilms J., Reynolds C.S., Begelman M.C., et al., 2001, MNRAS 328, L27

Woltjer L., 1959, ApJ 130, 38

Zdziarski A.A., Johnson W.N., Magdziarz P., 1996, MNRAS 283, 193

Zensus J.A., 1997, ARA&A 35, 607